Humanized substitutions of *Vmat1* in mice induce changes in amygdala-dependent behaviors associated with the evolution of anxiety in humans

Daiki X. Sato[1, #†], Yukiko U. Inoue[2†], Yuki Morimoto[2], Takayoshi Inoue[2], Nahoko Kuga[3], Takuya Sasaki[3, 4], Yuji Ikegaya[3, 5, 6], Kensaku Nomoto[7], Takefumi Kikusui[8], Satoko Hattori[9], Giovanni Sala[9], Hideo Hagihara[9], Tsuyoshi Miyakawa[9] and Masakado Kawata[1]*

[1]Graduate School of Life Sciences, Tohoku University, Sendai, Miyagi 980-8578, Japan
[2]Department of Biochemistry and Cellular Biology, National Institute of Neuroscience, National Center of Neurology and Psychiatry, Kodaira, Tokyo 187-8502, Japan
[3]Graduate School of Pharmaceutical Sciences, The University of Tokyo, 7-3-1 Hongo, Bunkyo-Ku, Tokyo 113-0033, Japan
[4]Precursory Research for Embryonic Science and Technology (PRESTO), Japan Science and Technology Agency (JST), 4-1-8 Honcho, Kawaguchi, Saitama 332-0012, Japan
[5]Center for Information and Neural Networks, National Institute of Information and Communications Technology, 1-4 Yamadaoka, Suita City, Osaka, 565-0871, Japan
[6]Institute for AI and Beyond, The University of Tokyo, Tokyo 113-0033, Japan
[7]Department of Physiology, Dokkyo Medical University, Mibu, Tochigi, 321-0293, Japan
[8]Department of Animal Science and Biotechnology, Azabu University, Kanagawa, Japan
[9]Division of Systems Medical Science, Institute for Comprehensive Medical Science, Fujita Health University, Toyoake, Aichi 470-1192, Japan
[#]Present address: Graduate School of Science, Chiba University, Chiba, 263-8522, Japan
[†]equally contributed
*email address of the corresponding author: kawata@tohoku.ac.jp
TEL +81-22-795-6688

Keywords: *Vmat1*, monoamine transporter, anxiety, amygdala, human evolution, CRISPR/Cas9

Abstract

The human vesicular monoamine transporter 1 (*VMAT1*) harbors unique substitutions (Asn136Thr/Ile) that alter monoamine uptake into synaptic vesicles. These substitutions are absent in all known mammals, suggesting their contributions to distinct aspects of human behavior modulated by monoaminergic transmission, such as emotion and cognition. To directly test the impact of these human-specific mutations, we introduced the humanized residues into mouse *Vmat1* via CRISPR/Cas9-mediated genome editing and examined changes at the behavioral, neurophysiological and molecular levels. Behavioral tests revealed reduced anxiety-related traits of *Vmat1*^{Ile} mice, consistent with human studies, and electrophysiological recordings showed altered oscillatory activity in the amygdala under anxiogenic conditions. Transcriptome analyses further identified amygdala-specific changes in the expression of genes involved in neurodevelopment and emotional regulation, which may corroborate the observed phenotypes. This knock-in mouse model hence provides compelling evidence that the mutations affecting monoaminergic signaling and amygdala circuits have contributed to the evolution of human socio-emotional behaviors.

Introduction

Recent years have seen a surge in the study revealing distinct human brain characteristics at the molecular, cellular, and circuit levels in both cortex and subcortical structures [1–4]. Differences in brain monoaminergic signaling are likely to be key factors conferring human attributes, as various monoaminergic pathways are involved in emotional regulation, memory consolidation, cognitive flexibility, and complex social behaviors [5–7]. Comparative studies have indeed demonstrated the distinct monoaminergic mechanisms in the human brain [2,8]. Moreover, diversification of monoaminergic mechanisms has been linked to the evolution of social behavior in non-human primates [9–12]. Thus, genetic differentiation of monoaminergic genes may underlie our unique emotional and social characteristics, such as empathy and altruism[2].

In line with these studies, we recently reported that the vesicular monoamine transporter 1 (*VMAT1*; also known as *SLC18A1*) gene has been under positive selection in the human lineage as evidenced by two amino acid substitutions (Glu130Gly and Asn136Thr) not shared by other primates [13]. The VMATs transport monoamine neurotransmitters into synaptic vesicles, thereby regulating the kinetics of synaptic transmission. There are two isoforms of VMAT, VMAT1 and 2, with the VMAT2 being highly expressed in the brain and widely studied [14,15]. In contrast, VMAT1 was previously thought to be expressed solely in the peripheral nervous system and chromaffin cells, and its functional importance in the CNS has only recently been implicated [16]. Our previous study showed that a new mutation at the 136th amino acid (136Ile) of *VMAT1* has emerged relatively recently in the course of human evolution,

73 and that the human-specific polymorphism Thr136Ile has likely been maintained by
74 balancing selection within non-African populations [13]. Moreover, fluorometric assays
75 demonstrated that these human-specific residues enhance monoamine neurotransmitter
76 uptake, suggesting the tendency of lower monoamine uptake in early hominids [17]. The
77 136Thr, the dominant variant across populations, is known to be marginally associated
78 with psychiatric diseases, such as bipolar disorder, depression and anxiety, as well as
79 with the neuroticism, a personality trait conferring greater risk of psychiatric disease [18–
80 20]. Thus, higher levels of depression and/or anxiety-like behaviors with 136Thr may
81 have been favored in our ancestors, while more recent selection may have led to the
82 emergence of 136Ile after the migration out of Africa and into harsher environments.
83 Although the evolution of *VMAT1* and its basic functions in the mammalian
84 CNS have been clarified, their contributions to unique human attributes are still unclear.
85 Here we examine the molecular, neurological, and behavioral changes in mice caused
86 by human-specific *VMAT1* mutations. We show that humanized *Vmat1* (*Vmat1*^{Ile})
87 induces amygdala-specific changes in gene expression and neuronal activity, reduces
88 anxiety-like behaviors under anxiogenic conditions and even enhances preference for
89 social novelty. These findings suggest that altered monoaminergic signaling in the
90 amygdala has contributed to the evolution of human emotional and social behaviors,
91 and the present work provides a new experimental strategy for evolutionary studies of
92 human emotions.
93
94

Results and discussion

Conservation of the 136th residue of VMAT1 across non-human vertebrates

To investigate the evolutionary significance of the 136th residue in human VMAT1 (hVMAT1), we first examined the conservation of this residue in a wide range of taxa in vertebrates. Multiple sequence alignments of VMAT1 among 236 vertebrate species revealed the unique evolution of this residue in the human lineage (Fig. 1a). Notably, we confirmed that all species but bicolor damselfish retain asparagine (Asn) at the 136th amino acid, while *Homo sapiens* is the only vertebrate species that carries the unique Thr136Ile (rs1390938) polymorphism.

Predicted effects of humanized residues on mouse VMAT1 structure and function

We then conducted *in silico* predictions of wild type mouse VMAT1 (mVMAT1) protein structure and the changes conferred by human substitutions (Fig. 1b). Like the hVMAT1 residue 136, we found out that the corresponding residue in mVMAT1 (133Asn) was located between the first luminal loop and the second transmembrane domain, suggesting a similar function. Given the evolutionary conservation across vertebrates and the difference in chemical properties between amino acids, the humanized mutations to mVMAT1, especially 133Asn to 133Ile, were predicted to have a significant impact on protein function (Table 1). Furthermore, the Asn133Ile mutation was also predicted to stabilize the protein structure as evidenced by greater folding free energy ($\Delta\Delta G$: 1.106 kcal/mol; Table 1) and to increase the flexibility of the loop domain (Fig. 1b), which possibly increases the efficiency of monoamine uptake.

117

118 **Generation of *Vmat1*-humanized mouse models by CRISPR/Cas9 genome editing**

119 In order to replace the 133Asn of mouse Vmat1 with Thr or Ile, we employed the
120 CRISPR/Cas9-mediated genome editing strategy (Fig. 2a). We selected a guide RNA
121 targeting the 133rd Asn codon in *Vmat1* exon 4 by using the web-based CRISPR design
122 tool to minimize off-target cleavage risk (Supplementary Table S1 and 2, see Methods
123 for details). By electroporating CRISPR components (*Vmat1* exon 4 crRNA, tracrRNA,
124 and Cas9 nuclease) along with the ssDNA donor containing the desired substitutions
125 into C57BL/6J fertilized eggs (Fig 2a, Supplementary Fig S1a), we successfully
126 generated 133Thr founder No.1 and 133Ile founder No.10 (Supplementary Fig. S1b, c
127 and d). After confirming the absence of off-target cleavages (Supplementary Fig. S2),
128 we crossed 133Thr founder No.1 and 133Ile founder No.10 with wild type (WT)
129 C57BL/6J mice to obtain heterozygous F1 generations, which were again verified to
130 possess the designed substitutions by Sanger sequencing. The homozygous mice were
131 further crossed after the F5 generations to obtain three humanized genotypes, Thr/Thr,
132 Thr/Ile, and Ile/Ile, in addition to WT, for behavioral, neurophysiological, and
133 transcriptomic analyses (Supplementary Fig. S3, see Methods).

134

135 **The human Ile substitution in mVMAT1 reduced behavioral anxiety**

136 We accordingly conducted comprehensive behavioral tests among the 20 sets of mice
137 including one of each genotype (*Vmat1*^{WT}, *Vmat1*$^{Thr/Thr}$, *Vmat1*$^{Thr/Ile}$, and *Vmat1*$^{Ile/Ile}$)
138 from the 1st batch at 9–55 weeks (see Supplementary Table S3 for detailed information

139 on age and the number of individuals used in each test). Detailed results were shown in
140 Fig. S4–19. Tests of social interaction (SI) between stranger mice of the same genotype
141 in a novel environment (one-chamber SI test) and of preference for a novel stranger
142 over a previously exposed stranger (now familiar) in Crawley's 3-chamber social
143 interaction (CSI) test revealed marginal differences in behavioral phenotypes between
144 mice with and without *Vmat1*^{Ile} (P = 0.062 for interactive effects of genotype (Ile) and
145 place, generalized additive model (GAM) with quasi-Poisson distribution; Fig. 3a,
146 Supplementary Fig. S9 and 10). In the CSI, *Vmat1*$^{Thr/Thr}$ mice significantly preferred
147 familiar to stranger mice ($P = 3.26\times10^{-4}$), while no such tendency was observed in
148 *Vmat1*^{Ile} mice (P = 0.759 for *Vmat1*$^{Thr/Ile}$ mice and (P = 0.195 for *Vmat1*$^{Ile/Ile}$ mice; Fig.
149 3a). Moreover, we found consistently lower levels of anxiety among *Vmat1*^{Ile} mice
150 across tests, including relatively greater preference for the (anxiogenic) light box during
151 the two-chamber light/dark transition (LD) test and for the center of an open field (OF)
152 (Supplementary Fig. S5 and 6).
153 To confirm a pervasive effect on specific behavioral domains by humanized
154 VMAT1, we constructed composite behavioral phenotype scores by summating
155 standardized scores on related tests (LD, OF, elevated plus maze (EP), and SI tests) and
156 compared the results among genotypes. We further conducted Structural Equation
157 Modeling (SEM) to investigate the effects of genotype on these composite scores. This
158 analysis revealed a significant effect of 133Ile on anxiety scores (R^2 = 0.15, $P = 8.7\times10^{-}$
159 ^{3}) but only marginal effects on locomotor activity (R^2 = 0.062, P = 0.053; Fig. 3b).
160 Anxiety levels were generally lower in *Vmat1*^{Ile} mice (P = 0.016, one-way ANOVA;

161 Fig 3c). These phenotype changes (i.e., a pattern in which *Vmat1*^{Thr} exhibits a similar
162 phenotype while *Vmat1*^{Ile} differs compared to *Vmat1*^{WT}) are in line with the *in silico*
163 prediction of differentiated transport function for the mVMAT1 133Ile (Table 1, Fig.
164 1b) likewise in the hVMAT1 136Ile [16,17] and previous studies demonstrating altered
165 fear/anxiety responses and psychopathological effects of the variant [16,20].
166 In addition to standard tests of anxiety, exploratory tendency, and locomotor
167 activity, we also performed a novel delayed reward task to evaluate the differences in
168 impulsivity between *Vmat1*$^{Thr/Thr}$ and *Vmat1*$^{Ile/Ile}$ mice (n = 10 for both genotypes, see
169 Methods for detailed experimental procedure; Supplementary Fig. S19a–c). Throughout
170 the test, there was no statistically significant difference in food preference between
171 genotypes (P = 0.50 for the first term, GAM with quasi-Poisson distribution;
172 Supplementary Fig. S19d). However, *Vmat1*$^{Ile/Ile}$ showed a lower preference for the
173 higher-calorie but delayed food reward than *Vmat1*$^{Thr/Thr}$ mice every test day from 5 to 9
174 except for day 6 compared to the basal level after habituation (day 4) (Supplementary
175 Fig. S19d). This finding may suggest that the *Vmat1*$^{Ile/Ile}$ mice are more impulsive, at
176 least initially, under this condition but contradicts an epidemiological study reporting an
177 association of 136Thr with maladaptive impulsivity [20]. Kim et al. (2018) reported that
178 the deletion of the D2 dopamine receptor (D2R) increased impulsive behavior in mice,
179 whereas restoration of D2R in the amygdala alone normalized impulsive behavior [21].
180 This is compatible with our results, as dopaminergic genes including *Drd2* were
181 downregulated in *Vmat1*$^{Ile/Ile}$ mice (see subsequent sections). The possible difference in
182 association of *VMAT1* genotype with impulsivity between humans and mice may stem

183 from functional connectivity changes in related neural circuits and warrants further
184 investigation.
185 Overall, these observations suggest that the 136Ile substitution may contribute
186 to uniquely human behavioral traits that have propelled both our technological progress
187 and adaptation to almost all ecosystems, namely high exploratory tendency and
188 relatively lower anxiety under threatening or novel conditions. Indeed, 136Ile allele
189 frequency increases along the migration route of modern humans [13], suggesting that the
190 exploratory tendency and/or boldness conferred by this mutation was advantageous for
191 survival. In this regard, *Vmat1*^{Ile} is analogous to the D4R polymorphism associated with
192 novelty-seeking behavior [22].
193
194 **Differential regulation of dopaminergic and neurodevelopmental genes in the**
195 **amygdala by *Vmat1* genotype**
196 We then conducted RNA-Seq analysis to investigate the effects of the four *Vmat1*
197 genotypes on gene expression patterns in three brain regions likely associated with the
198 behavioral phenotypes (prefrontal cortex, amygdala, and striatum) (n = 4 mice for each
199 genotype; see Supplementary Table S4 for detailed information on samples and reads).
200 Samples were obtained from mice exploring in a novel environment for 30 min. A total
201 number of 13,608 genes were assessed after excluding a putative amygdala sample
202 derived from a *Vmat1*$^{Thr/Thr}$ mouse due to possible sampling error (Supplementary Fig.
203 S20; see the detailed description in Methods). Principal component analysis revealed

204 distinct expression patterns among brain areas, but no obvious differences between
205 genotypes and ages (4 vs. 10 months) (Supplementary Fig. S20).
206 We thus screened for differentially expressed genes (DEGs) by pair-wise
207 comparisons between genotypes, which yielded a total of 80 DEGs exclusively in the
208 amygdala (Fig. 4a). A large proportion of these genes (56 out of 80) were differentially
209 expressed between *Vmat1*^{WT} and *Vmat1*$^{Ile/Ile}$ mice (Fig. 4a). The expression levels of
210 DEGs for each sample were shown in Supplementary Fig. S21. We then utilized the
211 correlations between composite anxiety scores and individual expression levels
212 (transcripts per million, TPM) of the detected amygdalar DEGs among a subset of 8
213 mice (n = 2 for each genotype). Particularly strong correlations were found for nine
214 genes, *Baz1a*, *Camk2n1*, *Ccdc114*, *Cldn1*, *Fsbp*, *Gdnf*, *Gm42608*, *Gsg1l*, and *KI* ($P <$
215 0.1; Fig. 4b, Supplementary Fig. S22). The DEGs were further examined for gene
216 ontology (GO) enrichment, which revealed significant overrepresentation of genes
217 involved in "behavior", "fear response", "response to amphetamine", "cardiac muscle
218 tissue development", or "cAMP catabolic process" (Table 2) between WT and Ile/Ile
219 mice, while no GO terms were enriched in DEGs for other genotype comparisons (as
220 there were few such genes). Moreover, gene expression patterns in the Ile mice
221 amygdala were significantly positively correlated with those of striata of transgenic
222 mouse models of Huntington disease ($P < 1.0 \times 10^{-28}$; Supplementary Table S5, Fig.
223 S23). Huntington disease (HD) is characterized by progressive behavioral and cognitive
224 deficits and caused by an expanded CAG repeat in the huntingtin (*HTT*) gene. It is
225 possible that the Ile mice recapitulate some dimensions of HD pathology, given that

226 dopamine (DA) signaling likely plays a significant role in HD, and the only current
227 FDA-approved drug for HD is a VMAT2 inhibitor, tetrabenazine [23].
228 To further characterize the biological pathways affected by *Vmat1* genotype,
229 we performed weighted gene correlation network analysis (WGCNA; Fig. 4c), which
230 revealed a co-expressing gene module (M1; Fig. 4c) significantly overrepresented in the
231 WT vs. Ile/Ile comparison (odds ratio = 3.79, $P = 2.88\times10^{-8}$ by Fisher's exact test) that
232 was negatively correlated with composite anxiety score. These genes include many
233 involved in adrenergic (*Adra2b*), dopaminergic (*Adcy5*, *Adora2a*, *Drd1*, *Drd2*, *Gnal*,
234 *Gng7*, *Gpr6*, *Gpr88*, *Pde1b*, *Pde1c*, *Pde7b*, *Pde10a*, *Pdyn*, *Penk*, *Ppp1r1b*, *Rasgrp2*,
235 *Rgs9* and *Tac1*), glutamatergic (*Grm4*), and serotonergic (*Htr1b*, *Htr1d*, *Htr1f*, and
236 *Htr4*) signaling pathways. Lohoff et al. reported that *Vmat1* KO affected DA signaling
237 in particular, with upregulation of D2R and downregulation of tyrosine hydroxylase
238 (TH) observed in both the frontal cortex and striatum [24]. Given the association between
239 *Vmat1* KO and decreased DA in the frontal cortex, we speculated that *Vmat1*$^{Ile/Ile}$ mice
240 would also exhibit downregulation of D2R and upregulation of TH compared to WT
241 mice. Indeed, D2R (along with many other dopaminergic pathway genes) was
242 downregulated in *Vmat1*$^{Ile/Ile}$ mice compared to WT mice. However, there were no
243 significant differences in TH expression among genotypes (Supplementary Fig. S24),
244 suggesting that the *Vmat1* Ile allele alters dopaminergic transmission but not DA
245 synthesis.
246 Sub-network analysis further detected another functional gene cluster
247 involved in neural development within the co-expressing module (cluster 2 in Fig. 4d).

248 Strikingly, three DEGs, *Foxp1*, *Foxp2*, or *Six3*, all of which are important regulators of
249 neural growth, were located in hubs connecting genes involved in postsynaptic
250 signaling (cluster 1) and neural development (cluster 2). Foxp1 (forkhead box protein
251 P1) is a transcription factor that regulates the development of various tissues including
252 the brain. Foxp1 is implicated in human language and social development. Foxp1
253 heterodimerizes with Foxp2, and a human-specific Foxp2 substitution is associated with
254 language impairment [25,26]. Moreover, Foxp1 mutations and haploinsufficiency are
255 associated with language impairment, intellectual disability, and autism [27–29]. Foxp2
256 also regulates D2R expression [30], extracellular DA levels [26], and the development of
257 dopaminergic neurons [31,32], while the cluster 2 genes *Dlx6*, *Ebf1*, *Isl1*, and *Six*3 are all
258 implicated in the development of striatal neurons that express DA receptors [33–35]. The
259 DEG *Sema5b*, a possible target of Foxp1 [36], encodes an inhibitory guidance cue for
260 neuronal axons that has also been shown to regulate synaptic connections in the
261 hippocampus [37]. The DEG *Kl* encodes the enzyme Klotho, which catalyzes the
262 activation of fibroblast growth factor (FGF) isoforms and has been shown protect
263 dopaminergic neurons against oxidative stress [38], while Wnt2 (also known as Irp) has
264 been found to increase dopaminergic neuron number by inducing the proliferation of
265 progenitor cells in the developing midbrain [39]. The differential expression of these genes
266 may also be related to the regulatory role of VMAT1 in hippocampal neurogenesis [40],
267 which emerging evidence suggests is associated with anxiety-like behavior [41,42]. Taken
268 together, the differential regulation of DA signaling by *Vmat1* genotypes may have
269 widespread effects on neural development and plasticity.

270

271 **The humanized mVMAT1 disrupted anxiety-associated theta band activity in the**

272 **basolateral amygdala**

273 Aforementioned behavioral and transcriptomic results suggest that the *Vmat1* genotype

274 influences anxiety-related neuronal activity patterns. Inspired by a previous report that

275 theta (4–12 Hz) oscillations in the medial prefrontal cortex (mPFC) and basolateral

276 amygdala (BLA) are specifically enhanced under anxiogenic environments such as the

277 open arms of an elevated plus maze (EP) and the center area of an OF [43,44], we next

278 performed simultaneous local field potential (LFP) recordings from the dorsomedial

279 prefrontal cortex (dmPFC) and BLA in freely moving mice during elevated plus maze

280 (EP) exploration (Fig. 5a; n = 11 dmPFC and 9 BLA electrodes from 5 *Vmat1*^{WT}, n = 6

281 and 6 electrodes from 4 *Vmat1*$^{Thr/Thr}$ and n = 10 and 7 electrodes from 4 *Vmat1*$^{Ile/Ile}$

282 mice). The histological confirmation of electrode positions and raw LFP signals were

283 shown in Fig. 5b and c, respectively. Power spectral analysis of WT mice revealed

284 lower 4–7 Hz power in both dmPFC and BLA during exploration of the EP open arms

285 compared to close arms, suggesting a relationship with anxiety-like behavior (Fig. 5d).

286 Further, the Granger causality test revealed the directionality of 4–7 Hz oscillations

287 from the mPFC to BLA (Fig. 5e; n = 20 electrode pairs from 5 *Vmat1*^{WT} mice),

288 consistent with anatomical evidence that the dmPFC preferentially projects to the BLA

289 [45,46] and that mPFC theta oscillations drive BLA neuronal activity [44]. Based on these

290 observations, we compared 4–7 Hz power in dmPFC and BLA among genotypes. Both

291 WT and *Vmat1*$^{Thr/Thr}$ mice exhibited significantly lower LFP 4–7 Hz signal power in

292 dmPFC and BLA under the anxiogenic condition of open arm exploration compared to
293 closed arm exploration, while *Vmat1*$^{Ile/Ile}$ mice showed no such consistent activity
294 pattern in the BLA (Fig. 5f), suggesting that anxiety-related neuronal mechanisms in the
295 dmPFC–BLA circuit are disrupted by the *Vmat1*$^{Ile/Ile}$ genotype.
296 Lohoff and colleagues reported that the Ile variant enhanced DA uptake and
297 increased amygdalar activity in response to threat-related stimuli in humans [16].
298 Additional studies are required to reveal the precise association between these LFP
299 changes and amygdalar output in *Vmat1*^{Ile} mice. In light of our behavioral results, we
300 suggest that *Vmat1*^{Ile} may promote the activity of neurons that dampen anxiety, such
301 those projecting from the BLA to the central amygdala [47,48].
302
303 **Amygdala-specific transcriptomic and neuronal changes associated with anxiety**
304 **imply intra- and inter-species differences in emotion and social behavior**
305 One of the major findings of this study is that *Vmat1* genotype affected transcriptomic
306 regulation and neuronal activity primarily in the amygdala. Given that amygdalar DA
307 signaling is a powerful modulator of fear and anxiety [49], these alterations in gene
308 expression and oscillatory neuronal activity likely contribute to the observed reduction
309 in anxiety-like behaviors among *Vmat1*^{Ile} mice compared to WT mice. The abnormal
310 neuronal activity pattern detected in the amygdala but not PFC of *Vmat1*^{Ile} mice may
311 stem from a difference in VMAT1 expression levels across the brain. Previous studies
312 verified that *VMAT1* mRNA and protein expression levels are relatively high in the
313 amygdala compared to other brain regions in both rats and humans [18,50]. Our

314 transcriptome analysis also revealed higher expression of *Vmat1* in the amygdala than in
315 the striatum ($P = 0.0097$, Dunnett's test; Supplementary Fig. S25). In contrast, *Vmat2*
316 expression was comparable across regions (Supplementary Fig. S25), indicating
317 distinctive regional regulation between subtypes as shown in a previous study [40].
318 Neuronal circuits within the amygdala store associations between
319 environmental cues and adverse stimuli as changes in synaptic strength, and these
320 modified circuits drive the expression of emotion-related behaviors and physiological
321 responses. Thus, the amygdala is a critical regulator of emotional and social behaviors
322 [51], and in fact amygdalar dysfunction is implicated in a number of neuropsychiatric
323 disorders [52–54]. Although it is an evolutionarily primitive brain region with relatively
324 well conserved gross structure and general function across species [48], recent studies
325 have provided evidence for more subtle structural and/or functional differences within
326 and among species potentially linked to differential regulation of monoaminergic
327 signaling via VMAT1. The size of the amygdala has been shown to correlate with
328 creativity [55] , mental state inference [56], and the size and complexity of social networks in
329 humans [57] and non-human primates [58]. The DA response in the medial amygdala
330 network is associated with mother‑infant bonding [59]. Collectively, these findings
331 strongly suggest a substantial contribution of the amygdala to evolution of the human
332 social brain by acting as a hub among brain networks associated with emotion,
333 cognition, and communication [60].
334 Given the limited number of samples and brain regions, there may be inter-
335 genotype differences in the transcriptome and neurological characteristics that have not

336 yet been detected. This might explain why we found little difference in the
337 transcriptome between *Vmat1*^{Thr} and *Vmat1*^{Ile} mice, unlike the results of the
338 neurological and behavioral studies. In the future, spatiotemporal transcriptomics and
339 electrophysiological recordings would thus be needed to solve this problem.
340
341 **A single substitution in humanized mouse models highlight molecular and**
342 **neurological evolution underlying human emotional traits**
343 Genetic deletion (KO) and overexpression have become predominant strategies for
344 examining the neurological, behavioral, and pathogenic functions of specific genes.
345 However, gene deletion and overexpression may alter the expression levels of many
346 additional genes, and thus the observed phenotype may be distinct from that induced by
347 target-specific pharmacological manipulations. The present study employed an
348 alternative "knock-in" strategy of a non-synonymous *Vmat1* mutation and succeeded in
349 capturing moderate differences in transcriptomic, neuronal, and behavioral phenotypes.
350 Noticeably, the variant evaluated is a human-specific substitution (i.e., Thr136Ile of
351 *VMAT1*) under selection that is not possessed by other mammals (Fig. 1a). This knock-
352 in model thus provides a unique opportunity to examine the molecular and neurological
353 mechanisms that distinguish human behavior from that of other primates. Such
354 extensive functional analysis of a single mutation has been limited to a few genes such
355 as *FOXP2* [26,61] and never for effects on emotional traits. To the best of our knowledge
356 [62], this is the first to suggest a new experimental strategy for studies on the evolution of
357 human brain mechanisms underlying emotion and related behavioral traits.

358 Recent genome-wide association studies (GWAS) on psychiatric disorders
359 such as depression [63] and schizophrenia [64], and on specific personality traits [65] have not
360 detected VMAT1 as a top hit despite alleged associations with the phenotypes under
361 study[20,66]. This may indicate that VMAT1 has a weaker influence on phenotype than
362 other significant loci, or that this gene must interact with other loci (epistasis) and/or
363 environmental factors (G × E interaction) for measurable effects on phenotype. Such
364 dependence on other genes or external factors could obscure phenotypic associations of
365 VMAT1 evaluated by conventional approaches of GWAS. In fact, we found that a
366 single amino acid substitution (Asn133Ile) altered the expression of 56 genes within the
367 amygdala, any or all of which may contribute to the observed changes in behavioral
368 phenotype. The effects of various environmental factors (which were largely controlled
369 in this experiment through group housing and shared dams) and DEGs on these
370 behavioral and neurological phenotypes would warrant further study.
371
372 **Concluding remarks**
373 The present study utilized the CRISPR/Cas9 system in mice to demonstrate that the
374 human *VMAT1* 136Ile mutation can markedly alter emotional behavior, leading to a less
375 anxious and less neophobic behavioral trait. This phenotypic variation might help
376 explain our unique penchant for exploration as well as our complex social relationships.
377 We additionally show that these behavioral changes stem at least in part from the ripple
378 effects of this humanized substitution on gene expression and neuronal activity within
379 the amygdala. First, comprehensive behavioral tests confirmed a similar behavioral

380 effect of this mutation in mice as observed in humans, where *Vmat1*^{Ile} (*Vmat1*$^{Thr/Ile}$ and
381 *Vmat1*$^{Ile/Ile}$) is associated with lower levels of anxiety. Second, electrophysiological
382 recordings revealed altered neuronal oscillation patterns in the amygdala of *Vmat1*$^{Ile/Ile}$
383 mice under anxiogenic conditions (i.e., open arms of the elevated plus maze), which
384 likely contributes to the behavioral phenotype. Third, transcriptome analysis of the
385 *Vmat1*$^{Ile/Ile}$ mouse amygdala revealed altered expression of several dozen genes
386 implicated in neural development and emotional control, consistent with the observed
387 behavioral changes. Collectively, our results exemplify the utility of this knock-in
388 mouse model for studies on human brain evolution and the mechanisms underlying
389 emotions and neuropsychiatric diseases.
390

391 **Methods**

392 **Multiple sequence alignments and phylogenetic tree of *VMAT1***

393 Two hundred sixty-three orthologous sequences of vertebrate *SLC18A1* (*VMAT1*) were
394 obtained from Ensembl101. After aligning the sequences using webPRANK [67] with
395 default parameters, we calculated the proportions of amino acids identical to the human
396 *VMAT1* within aligned protein regions. Sequences with < 50% identity were then
397 excluded. In the case of multiple sequences for a given species, that with the highest
398 proportion of identical amino acids to human *VMAT1* was . A phylogenetic tree was
399 then constructed from the 236 species sequences with > 50% identity to human *VMAT1*
400 using IQTREE v2.1.1 [68] with the "-nt AUTO" setting, including the Neanderthal
401 sequence, which we constructed by replacing 136Ile in the human reference sequence
402 with 136Thr. Phylogenetic relationship was visualized using iTOL v5.6.3 [69] through a
403 web interface (https://itol.embl.de). Animal silhouettes were obtained from phylopic
404 (http://phylopic.org/) under Public Domain license.

405

406 ***In silico* prediction of mVMAT1 structure and tolerance of mutated residues**

407 Homology modeling of the mouse VMAT1 (mVMAT1) protein structure was
408 performed using the SWISS-MODEL [70] web server (http://swissmodel.expasy.org). The
409 human organic anion transporter MFSD10 (PDB: 6s4m.1.A) was selected as the best
410 template, with sequence identity of 17.04 (verified June 2020) and QMEAN score of –
411 8.40 according to SWISS-MODEL. The predicted 3D structure of mVMAT1 was
412 visualized using PyMOL 2.4.1 (DeLanoScientific, San Carlos, CA). Provean v1.1.3 [71]

413 and SIFT [72] were used to estimate the intolerance for individual amino acid mutations
414 introduced in mVMAT1 based on the evolutionary conservation and the chemical
415 properties of the exchanged residues. The computations were made using the Provean
416 web server (http://provean.jcvi.org/protein_batch_submit.php?species=mouse; last
417 accessed June 2020). A mutation is predicted as deleterious (i.e., likely to affect its
418 protein function) when the Provean score is smaller than −2.5 or the SIFT score is
419 smaller than 0.05. Furthermore, we used DynaMut [73] to evaluate the effects of
420 humanized mutations on the stability and flexibility of VMAT1 protein structure.
421 Briefly, DynaMut enables accurate assessment of mutation impact on protein stability
422 by implementing and integrating well established normal mode approaches with graph-
423 based signatures in a consensus predictor [73]. Here we focused on two measurements: 1)
424 folding free energy (ΔΔG), an index of the difference in stability between WT and
425 mutant proteins in which positive values represent increased stability of the mutant, and
426 2) Δ vibrational entropy energy (ΔΔSVib ENCoM), a per-site index of the difference in
427 flexibility between WT and mutant proteins. Calculations were conducted using a web
428 server (http://biosig.unimelb.edu.au/dynamut/).
429

430 **Ethical approvals**

431 All animal care protocols and experiments were conducted according to guidelines by
432 the Animal Care and Use Committee of the National Institute of Neuroscience, National
433 Center of Neurology and Psychiatry (approval number: 2017005, 2020007), the Animal
434 Experiment Committee of Fujita Health University (approval number: APU19063), and

435 the Experimental Animal Ethics Committee of the University of Tokyo (approval
436 number: P29-14). All efforts were made to minimize the suffering of mice.
437
438 **Generation of *Vmat1*-humanized mouse models by CRISPR/Cas9 genome editing**
439 *Preparation of the CRISPR components and donor DNAs*
440 The target region within the mouse *Vmat1* exon 4 was first analyzed by using the web-
441 based CRISPR design tool CRISPOR [74] (http://crispor.org), to select a guide RNA
442 sequence for replacing mouse 133Asn with 133Thr or 133Ile via the CRISPR/Cas9
443 system with minimal risk of off-target cleavages. Then, two parts of the CRISPR guide
444 RNA, crRNA and tracrRNA (shown in Fig. 2a, Supplementary Fig. S1a, and
445 Supplementary Table S1), were chemically synthesized and purified by reversed-phase
446 column chromatography (FASMAC, Japan). Recombinant Cas9 protein (EnGen Cas9
447 NLS from *Streptococcus pyogenes*) was purchased from New England Biolabs
448 (Ipswich, MA). The single-strand DNA (ssDNA) donors containing the humanized
449 substitution and the restriction enzyme recognition sites flanked by 42–50 bp homology
450 arms (Supplementary Table S1) were subsequently designed and chemically
451 synthesized by Eurofins Genomics (Tokyo, Japan). In addition to the intended
452 humanization, the synonymous substitutions depicted in Fig. 2a were introduced near
453 the 133rd site to prevent unwanted re-editing. For 133Thr substitution, an *Eco*RI site
454 was synonymously integrated into the protospacer adjacent motif (PAM) sequence to be
455 destroyed. An *Fsp*I site was similarly incorporated within the guide RNA target
456 sequence for the 133Ile allele. These synonymous substitutions also made the

457 genotyping procedure much easier by eliminating the need for laborious sequencing
458 (Fig. 2b).
459
460 *Electroporation of mouse one-cell embryos*
461 One-cell-stage embryos were collected by *in vitro* fertilization using C57BL/6J super-
462 ovulated females (Charles River, Japan) and stud males. The guide RNAs, Cas9
463 proteins, and the donor ssDNAs were electroporated into mouse zygotes following the
464 standard protocol [75] to obtain founder knock-in mice (Supplementary Fig S1a).
465
466 *PCR Genotyping and sequencing analyses*
467 Genomic DNAs were prepared from the newborn mouse tail by treatment with
468 proteinase K in Lysis Buffer. The 133Thr and 133Ile knock-in founders were screened
469 by PCR-RFLP assay (Supplementary Fig. S1c). Briefly, PCR products were amplified
470 using the primer pairs depicted in Fig. 2a (also listed in Supplementary Table S1) and
471 then digested by *Eco*RI or *Fsp*I, respectively. For founders and F1 generations, PCR
472 products were also analyzed by Sanger sequencing to confirm the correct substitution
473 allele. After that, PCR-RFLP could be used reliably for genotyping of subsequent
474 generations.
475
476 *Off-target analyses of founder mice*
477 To exclude the possible side effects from off-target cleavages, the genomic DNAs
478 extracted from the founder mice (133Thr No.1 and 133Ile No.10, shown in

479 Supplementary Fig. S1c and d) were analyzed by Sanger sequencing. We employed
480 CRISPOR [74] (http://crispor.org) to predict potential off-target candidate loci, and the 12
481 loci identified (Supplementary Table S2) were amplified by PCR using the primers
482 listed in Supplementary Table S1 and sequenced (results are shown in Supplementary
483 Fig. S2).
484
485 *Preparation of humanized mouse models for behavioral tests, transcriptome analyses,*
486 *and neurophysiological analyses*
487 After confirming the absence of off-target cleavages, 133Thr founder No.1 and 133Ile
488 founder No.10 were crossed with WT C57BL/6J mice to obtain heterozygous F1
489 generations, which were again verified to possess the designed substitutions by Sanger
490 sequencing. Homozygous 133Thr and 133Ile mice after F2 generations were then
491 selected and maintained. For behavioral tests, F5 or F6 homozygous mice were crossed
492 to obtain Thr/Thr, Thr/Ile, and Ile/Ile genotypes. In addition, C57BL/6J WT males and
493 females carrying the Asn/Asn genotype were crossed to supply control mice. To
494 eliminate differences in rearing environment, newborn males of the 4 genotypes
495 (Asn/Asn, Thr/Thr, Thr/Ile, and Ile/Ile) were grouped in sets and nursed by the same
496 mothers. At 4 weeks old, 20 sets of 4 males, one of each genotype, were weaned and
497 housed in 20 separate cages. Behavioral tests were conducted between 9 and 55 weeks
498 of age as indicated (Supplementary Table S3). A subset of these mice (1st batch) was
499 also used for transcriptome analyses at 42–45 weeks. Likewise, 8 sets of mice (2nd

500 batch) including all 4 genotypes were generated and used for transcriptome analysis at
501 15 weeks and electrophysiological recordings at 16–24 weeks.
502
503 **Animal care and experimental conditions for behavioral tests**
504 Animals were housed in groups of four individuals of each genotype under a 12 h
505 light/dark cycle (7:00 AM to 7:00 PM) with ad libitum access to food and water. Adult
506 male mice were used in all tests to eliminate the behavioral effects of the estrus cycle.
507 Behavioral tests were performed between 8:00 AM and 6:00 PM in a room maintained
508 at 23°C ± 2°C. Mice were habituated to this experimental room for a minimum of 30
509 min before testing. The composition of cohorts and ages of the mice for every
510 experiment are summarized in Supplementary Table S3. All devices used were cleaned
511 with diluted hypochlorite solution or 70% ethanol after each trial to prevent influences
512 from residual olfactory cues. To minimize the impact of one test on subsequent tests in
513 individual mice, behavioral assessments were conducted in the following order after
514 general health and neurological screens: light/dark transition, open field, elevated plus
515 maze, hot plate, social interaction in a novel environment, rotarod, Crawley's 3-
516 chamber social interaction test, startle response/prepulse inhibition, Porsolt forced
517 swim, T-maze, Barnes maze, tail suspension, fear conditioning, and home cage social
518 interaction tests. All behavioral tests were conducted at intervals of at least one day.
519
520 **Behavioral battery tests**
521 *General health and neurological screens (GHNS)*

522 The presence of whiskers and bald patches was checked daily to ensure the health status
523 of mice [76]. The righting, whisker touch and ear twitch reflexes were also evaluated to
524 insure age-appropriate neurological function. Body weight and rectal temperature were
525 measured. In addition, neuromuscular function was assessed by grip strength and wire
526 hanging tests. Briefly, grip strength was measured using a grip strength meter (O'Hara
527 & Co., Tokyo, Japan). The mouse was positioned to spontaneously grasp a wire grid by
528 the forelimbs and then pulled backward by the tail until wire release. The peak force
529 was recorded in Newtons (N). Each mouse was tested three times, and the greatest value
530 obtained was used for further analyses. In the wire hanging test, a mouse was placed on
531 a wire mesh at the top of the apparatus (O'Hara & Co.), and the wire mesh was then
532 gently turned upside down. The mouse gripped the wire in order not to fall off, and the
533 latency to fall was recorded with a 60 s cut-off time.
534
535 *Light/dark transition (LD)*
536 The light/dark transition test was conducted to measure anxiety level as previously
537 described [77]. The apparatus consisted of two equal-sized plastic boxes (20 × 20 cm), one
538 illuminated (390 ± 20 lx) and the other dark (< 2 lx), separated by a central partition
539 plate with a small 3 × 5 cm opening allowing the mouse to transit from one box to the
540 other. A mouse was first placed in the dark box and allowed to freely explore the
541 apparatus for 10 min. The time to first entry into the light box, time spent in the light
542 box, number of transitions between boxes, and distances traveled in light and dark

543 boxes were measured using Image LD software (see "Image analysis of behavioral
544 tests").
545
546 *Open field (OF)*
547 Locomotor activity and explorative tendency were measured using an open field
548 apparatus (40 × 40 × 30 cm; Accuscan Instruments, Columbus, OH) as described
549 previously [78]. The test chamber was illuminated at 100 ± 5 lx. A mouse was placed in
550 the corner of the apparatus and total distance traveled (cm), time spent in the center area
551 (20 × 20 cm), vertical activity, and stereotypic counts over 120 min were recorded by
552 the VersaMax system and analyzed using Image OF software (see "Image analysis of
553 behavioral tests").
554
555 *Elevated plus maze (EP)*
556 An elevated plus-maze test was conducted as previously described [79]. The apparatus
557 consisted of two open arms (25 cm long × 5 cm wide) crossing two enclosed arms of
558 identical dimensions but with 15-cm high transparent walls, all connected by a central
559 platform. The entire apparatus was elevated 50 cm above the floor and illuminated
560 uniformly at 100 lx. A mouse was placed at the center of the maze, facing one of the
561 closed arms and allowed to freely explore for 10 min. Number of open and closed arm
562 entries, distances traveled, proportions of entries into open arms, and proportions of
563 time spent in open arms were measured using Image EP software (see "Image analysis
564 of behavioral tests").

565

566 *Hot plate (HP)*

567 Pain sensitivity was measured by the hot plate test. A mouse was placed on a 55°C hot

568 plate (Columbus Instruments, Columbus, OH), and latency to escape from the plate was

569 recorded with a 15-s cut-off time.

570

571 *Social interaction in a novel environment (SI)*

572 The social interaction test in a novel environment test (one-chamber social interaction

573 test) was performed as described previously [76]. Two mice of the same genotype but

574 reared in different cages were placed together in a box (40 × 40 × 30 cm) and allowed to

575 explore freely for 10 min. Mouse behaviors were recorded with a CCD camera. The

576 total duration of contact, total number of contacts, total duration of active contact, mean

577 duration per contact, and total distance traveled were measured automatically using

578 Image SI software (see "Image analysis of behavioral tests"). Active contact was

579 defined as maintained contact while either mouse traveled more than 10 cm between

580 two successive image frames acquired once per second.

581

582 *Rotarod (RR)*

583 Motor coordination and motor learning were examined using an accelerating rotarod

584 (UGO Basile, Comerio, VA, Italy). The latency to fall from the rod was recorded during

585 three daily trials conducted on 2 consecutive days (3 × 2 trials). During each trial, rod

586 speed was increased from 4 to 40 rpm over the 5-min test period.

587

588 *Crawley's 3-chamber social interaction (CSI)*

589 Crawley's 3-chamber social interaction test was performed to measure sociability and
590 social novelty preference [78]. The experimental apparatus was a 41 × 62 cm rectangular
591 non-transparent gray Plexiglas box separated into three equal-sized chambers (20 × 40
592 cm) by transparent Plexiglas plates with small openings allowing mice to freely transit
593 from one chamber to another. One wire cylinder-shaped cage was placed in the corner
594 of each side chamber. Tested mice (aged 16–19 weeks, see Table S2) were first allowed
595 to freely explore the chambers for 10 min as a habituation period. A stranger mouse was
596 then placed randomly in one of the side-chamber wire cages and the tested mouse was
597 again allowed to freely explore the chambers for 10 min. In a final step, a second
598 stranger mouse was placed in the wire cage in the opposite side chamber, and the tested
599 mouse was again allowed to freely explore the chambers for 10 min. Number of
600 contacts and interaction times with strangers 1 and 2 were recorded using Image CSI
601 software (see "Image analysis of behavioral tests").

602

603 *Startle response / prepulse inhibition (PPI)*

604 Sensory-motor integration was tested by a prepulse inhibition test [76], which measures
605 the effect of an audible pre-tone (prepulse) of variable intensity on the startle response
606 to a louder pulse. The system used for the detection of startle reflexes (O'Hara & Co.)
607 consisted of four standard cages placed on a movement sensor within sound-attenuated
608 chambers with fan ventilation. Before each testing session, acoustic stimuli and

609 mechanical responses were calibrated using devices supplied by the manufacturer. A
610 test session was composed of 6 different trial types: two startle stimulus-only trials (110
611 or 120 db) and four prepulse inhibition trials (74 or 78 db prepulses delivered prior to a
612 110 or 120 db startle). Six blocks of the six trial types (i.e., 36 trials in total) were
613 conducted, with each trial type presented once in pseudorandom order within each
614 block. The PPI (%) was calculated for each trial type according to the following
615 equation: {[(startle amplitude of trial without prepulse) – (startle amplitude of trial with
616 prepulse)]/(startle amplitude of trial without prepulse)} × 100.
617
618 *Porsolt forced swim (PS)*
619 The Porsolt swim test was performed as previously described [76]. The apparatus
620 consisted of four Plexiglas cylinders (12 cm diameter × 22 cm height) filled with water
621 (room temperature) up to a height of 7.5 cm. Four mice (a set) were placed individually
622 in each cylinder, and images were captured at two frames per second for 10 min.
623 Swimming distance and immobility time (% of total) were recorded automatically using
624 Image TS software (see "Image analysis of behavioral tests").
625
626 *Tail suspension (TS)*
627 Mice were suspended 30 cm above the floor in a visually isolated area by adhesive tape
628 placed approximately 1 cm from the base of tail. Behavior during suspension was
629 recorded for 10 min using Image TS software (see "Image analysis of behavioral tests").
630

631 *T-maze (TM) forced alteration*

632 A T-maze forced alternation task was performed as previously described [80]. The T maze
633 was constructed of three white plastic runways with walls 25-cm high (O'Hara & Co.)
634 partitioned into 6 areas by sliding doors. The stem of the "T" was divided into a start
635 compartment area S1 at the intersection with the arms and a main area S2 (13 × 24 cm).
636 Similarly, the T arms were divided into passageway areas P1 and P2 with S1 and main
637 areas A1 and A2 (11 × 20.5 cm). Each trial consisted of one forced run followed by one
638 free run. First, the mouse was placed in S2 and forced to proceed in one direction (S2 →
639 A2 → P2 → S1, or S2 → A1 → P1 → S1) by opening the doors successively. After
640 returning to S1 and a set inter-trial delay, mice were then allowed to choose to enter A1
641 or A2. If the mouse chose the opposite direction from the previous forced run, it was
642 counted as a correct response, while if the mouse chose the same direction as the
643 previous run, it was counted as an incorrect response. After 30 practice trials (10 per
644 day for 3 consecutive days), trials with delay (4 trials with 3-s delays and 2 trials each
645 with 30-, 60-, and 120-s delays) were conducted for 3 consecutive days. Data were
646 acquired and sliding doors controlled automatically using Image TM software (see
647 "Image analysis of behavioral tests").

648

649 *Barnes maze (BM)*

650 Spatial learning, spatial memory, and behavioral flexibility were tested using the Barnes
651 maze as described previously [78]. The maze was a circular whiteboard (1m in diameter)
652 with 12 holes equally spaced around the margin and elevated 81.5 cm from the floor

653 (O'Hara & Co.). A black plastic box (17 × 13 × 7 cm) lined with paper cage bedding
654 was positioned under one of the holes (the target). The board position of the target (1–
655 12) was constant for a given mouse but randomly assigned across individuals. The
656 apparatus was illuminated at 800 lx or more. The board was rotated daily so that the
657 spatial location of the target changed relative to distal visual room cues while proximal
658 cues were held constant. A training trial was conducted per day over 20 days until 24
659 trials were completed in total before the 1st probe test. Each trial lasted a maximum of 5
660 min, and was completed when the mouse entered into the black plastic box. Probe tests
661 were conducted for 3 min without the black plastic box one day or one month after the
662 final training trial. The number of errors, latency and distance traveled to reach the
663 target hole for the first time, the number of omission errors and time spent around each
664 hole were recorded by Image BM software (see "Image analysis of behavioral tests").
665
666 *Fear conditioning (FZ)*
667 Contextual and cued fear conditioning tests were conducted and analyzed as described
668 in a previous study [76]. Mice were placed in a transparent acrylic chamber (26 × 34 × 33
669 cm, O'Hara & Co.) with 55 dB ambient white noise and 100 lx illumination. In the
670 conditioning session, the conditioned acoustic stimulus (CS, 55 dB) was presented for
671 30 s at three times (2, 4, and 6 min), and a mild foot shock (2 s, 0.3 mA) was presented
672 as the unconditional stimulus (US) at the end of each CS. One day after the conditioning
673 session, contextual fear was measured in the same chamber, while cued fear was
674 measured thereafter in a triangular box (33 × 33 × 33 cm) constructed of white opaque

675 Plexiglas. Mice were placed in the chamber for 3 min with neither CS nor US presented.
676 Thereafter, the CS (55 dB) was presented for the last 3 min and images were captured at
677 1 frame per second. Each pair of successive frames in which the mouse moved was
678 measured. When this measure was below a certain threshold (20 or 30 pixels), the
679 mouse was considered to be "freezing"; alternatively, when this measure equaled or
680 exceeded the threshold, the behavior was considered "non-freezing". "Freezing" that
681 lasted less than 2 s was not included in the analysis. Data acquisition, control of stimuli
682 (i.e., tones and shocks), and data analysis were conducted automatically using Image FZ
683 software (see "Image analysis of behavioral tests").
684
685 *Home cage social interaction test (HCSI)*
686 The 24-hour home cage locomotor activity and social interaction test was conducted as
687 previously described [81] for one continuous week. The monitoring system included a
688 standard home cage (29 × 19 × 13 cm) with filtered cage top and an infrared video
689 camera (O'Hara & Co.). Two mice of the same genotype that had been housed
690 separately were placed together in the home cage and locomotor activity and social
691 behavior monitored by video. Social interaction was measured by counting the number
692 of "particles" (tracers for each mouse) detected in each frame, with two separate
693 particles indicating no contact and one particle indicating physical contact (i.e., because
694 the tracking software could not distinguish two separate bodies). Data acquisition and
695 analysis were conducted using Image HA software (see "Image analysis of behavioral
696 tests")

697

698 **Delayed reward task**

699 Following these comprehensive behavioral tests, we conducted an original delayed
700 reward task to evaluate the impulsivity of *Vmat1*$^{Thr/Thr}$ and *Vmat1*$^{Ile/Ile}$ mice (n = 10 for
701 both genotypes). In brief, a mouse was housed in a cage (22.5 × 32.5 × 21 cm; FDB-
702 300W/FDL-8D, Melquest, Toyama, Japan) with controlled access to two separate
703 feeding trays for 16 days. Consumption of normal food (3.57 kcal/g; CRF-1, Oriental
704 Yeast Co., Ltd., Tokyo, Japan) and high-calorie food (Banana chip containing 5.42
705 kcal/g; 4515996091582, KALDI COFFEE FARM, Tokyo, Japan), considered small and
706 large rewards, respectively, were measured daily by weighing the feeding trays. After
707 habituating mice to this system for 4 days with ad libitum access to both foods, we
708 programmed feeding tray access so that the normal food was provided for the first 45
709 min and high-calorie food provided only for the last 15 min of the three 1-h daily
710 feeding time (7:00–8:00 PM, 10:00–11:00 PM, and 1:00–2:00 AM) for 6 consecutive
711 days. Under such delayed reward conditions, consumption of the lower-calorie food is
712 considered an impulsive behavior (i.e., does not maximize reward). Furthermore, to
713 maximize the impulsivity, we set a fasting day after the 6 days of delayed feeding while
714 monitoring animal weights (so as not to jeopardize the animal's health) and conducted
715 the same test again for 5 days.

716

717 **Image analysis of behavioral tests**

718 We developed in-house programs to analyze the imaging data acquired for many of
719 these behavioral tests (Image LD, Image OF, Image EP, Image SI, Image CSI, Image
720 TS, Image TM, Image BM, Image FZ, and Image HA) based on ImageJ (U.S. National
721 Institutes of Health; available at https://imagej.nih.gov/ij/) and modified for each test by
722 Tsuyoshi Miyakawa (available through O'Hara & Co.).
723

724 **Statistical analyses and Structural Equation Modeling (SEM)**

725 Group means were compared by paired sample *t*-test, unpaired Student's *t*-test, one-way
726 ANOVA, or pair-wise *t*-test with FDR correction by the Benjamini-Hochberg method
727 as indicated using R 4.0.2. We obtained comprehensive metrics for two major domains
728 of mouse behavior, activity and anxiety, by standardizing, normalizing, and combining
729 sets of related behavioral scores. Total distances traveled in LD, OF, EP, SI, and CSI
730 were used as indices for activity, while time in the light compartment of the LD shuttle
731 box, duration in the central area of the OF, time spent in open arms of the EP, and total
732 duration of active contacts in the SI were used as indices of anxiety. To further confirm
733 the effects of *Vmat1* genotype on the behavioral composites and to enhance statistical
734 power and improve reliability, we used Structural Equation Modeling (SEM) [82]. The
735 SEM model included a measurement model and a regression model. The measurement
736 model consisted of two latent factors grouping tests of locomotor activity and anxiety-
737 like behavior, which were assessed by the same metrics above. The regression model
738 evaluated the effect of genotype on the two latent factors. In the best fitted model,
739 genotype was labeled by the presence of Ile allele as follows: $Vmat1^{WT} = 0$, $Vmat1^{Thr/Thr}$

740 = 0, *Vmat1* $^{Thr/Ile}$ = 1, and *Vmat1* $^{Ile/Ile}$ = 1. Goodness of model fit was evaluated by
741 normed Comparative Fit Index (CFI), Root Mean Square Error of Approximation
742 (RMSEA), and the Standardized Root Mean Square Residual (SRMR) and significance
743 of paths was tested by *t*-test. Normalization of behavioral scores and SEM were
744 performed using the *bestNormalize* and *lavaan* packages in R, respectively. Availability
745 of the data and codes used are described in the section **Availability of data and**
746 **materials**.
747
748 ***In vivo* electrophysiological recordings**
749 *Subjects*
750 Five male WT C57BL/6J mice (16–20 weeks old, SLC Shizuoka, Japan) with
751 preoperative weights of 20–30 g as well as four male *Vmat1*$^{Ile/Ile}$ mice (16–20 weeks
752 old) and four male *Vmat1*$^{Thr/Thr}$ mice (20–24 weeks old) obtained from the 2nd batch
753 were implanted with intracranial electrodes for *in vivo* electrophysiological recordings.
754 The animals were housed under a 12 h/12 h light/dark schedule with lights on at 7:00
755 AM prior to surgery.
756
757 *Surgery*
758 Animals were anesthetized with isoflurane gas (1%–3%) and 1-mm diameter circular
759 craniotomies were made using a high-speed drill at the target coordinates. For local
760 field potential (LFP) recordings, an array of 3 immobile tetrodes was stereotaxically
761 implanted above the dmPFC (2.00 mm anterior and 0.50 mm lateral to bregma) at a

762 depth of 1.40 mm and an array of 4 tetrodes was implanted in the amygdala (0.80 mm
763 posterior and 3.00 mm lateral to bregma) at a depth of 4.40 mm using guide cannulae.
764 The tetrodes were constructed from 17-μm diameter polyimide-coated platinum–iridium
765 (90/10%) wire (California Fine Wire, Grover Beach, CA), and the individual electrode
766 tips were plated with platinum to lower the impedance to 200–250 kΩ. Stainless steel
767 screws were implanted on the skull attached to the brain surface to serve as
768 ground/reference electrodes. To prevent brain tissue drying at the implant sites, a
769 dummy cannula was inserted through the guide cannula and both covered by a cap. The
770 entire recording device was secured to the skull using stainless steel screws and dental
771 cement. After all surgical procedures were completed, anesthesia was discontinued, and
772 the animals were allowed to awaken spontaneously. Following surgery, each animal
773 was housed in a separate transparent Plexiglas cage with free access to water and food
774 for at least 7 days before recordings.
775
776 *Electrophysiological recording*
777 The mouse was connected to the recording equipment via a digitally programmable
778 amplifier (Cereplex M, Blackrock Microsystems, Salt Lake City, UT) placed close to
779 the animal's head. For recording electrophysiological signals, the EIB of the microdrive
780 array was connected to a Cereplex M digital headstage, and the digitized signals were
781 transferred to a Cereplex Direct data acquisition system. Electrical signals were sampled
782 at 2 kHz and low-pass filtered at 500 Hz. The animal's moment-to-moment position
783 was tracked at 15 Hz using a video camera attached to the ceiling.

784

785 *Elevated plus maze (EP)*

786 The elevated plus maze used during electrophysiological recording was made of ABS
787 resin and consisted of a central square (7.6 × 7.6 cm) and four arms (each 28 cm long ×
788 7.6 cm wide), two open arms with no railing and two closed arms enclosed by
789 transverse walls (15 cm in height). The maze was elevated 30 cm from the floor and
790 illuminated with two 32-W fluorescent overhead lights, which produced light intensities
791 of 250 ± 20 lx and 170 ± 20 lx in the open and closed arms, respectively. In a recording
792 session, a mouse was placed in the center of the central square facing an open arm and
793 allowed to explore the maze apparatus for 10 min.

794

795 *Confirmation of electrode locations by histological analysis*

796 The mice were overdosed with isoflurane, perfused intracardially with 4%
797 paraformaldehyde (PFA) in phosphate-buffered saline (PBS, pH 7.4), and decapitated.
798 After dissection, the brain was fixed overnight in 4% PFA/PBS and then cryoprotected
799 by successive overnight incubations in 20% sucrose and 30% sucrose in PBS. Frozen
800 coronal sections (100 μm) were cut using a microtome, mounted, and processed for
801 cresyl violet staining. Briefly, slices were rinsed in water, stained with cresyl violet, and
802 coverslipped with Permount. The positions of all electrodes were confirmed by
803 identifying the corresponding electrode tracks in histological tissue sections.

804

805 **Extraction of RNA and RNA sequencing**

806 Total RNA was extracted from the prefrontal cortex, amygdala, and striatum of four
807 mice per genotype (two 4-month-old and two 10-months-old individuals from batches 1
808 and 2), yielding 48 samples in total. Cage mates were selected for sequencing when
809 possible (see Supplementary Fig. S3 and Table S4 for detailed sampling information).
810 Briefly, mice were habituated to a novel cage for 30 minute and then decapitated under
811 anesthesia. The indicated brain regions were then isolated using a mouse brain atlas [83]
812 by the same experimenter. The extracted tissues were homogenized in BioMasher
813 Standard (TaKaRa, Shiga, Japan) and total RNA isolated using the RNeasy® Plus Mini
814 Kit (Qiagen, Hilden, Germany). RNA concentration and purity were assessed using a
815 Nano-Drop® ND-1000 spectrophotometer (Thermo Scientific, Waltham, MA), and
816 total RNA integrity quantified by the Agilent 2100 Bioanalyzer (Agilent Technologies,
817 Santa Clara, CA). From the 48 RNA samples, 48 cDNA libraries were prepared and 100
818 bp paired-end reads were sequenced on a DNBSEQ platform at the Beijing Genomics
819 Institute (BGI, Hong Kong, China). A total of 2,344,530,700 raw sequencing reads were
820 generated (24–25 million read pairs per sample; Supplementary Table S4) and used for
821 gene expression profiling.
822
823 **Data processing**
824 The raw reads were quality checked, trimmed, and filtered using fastp 0.20.0 [84],
825 yielding 20–21 million filtered reads (Supplementary Table S4). STAR v2.7.5c [85] was
826 then used for mapping the reads to the reference mouse genome (GRCm38.p6). We
827 assigned reads to the Ensembl100 annotation and generated fragment counts by the

828 featureCounts utility of the Subread package (v1.6.3) in R [86].We obtained reads with
829 mapping quality above 20 (essentially uniquely mapped reads) and only pairs that were
830 properly aligned on the same chromosome. The fragment counts were then used to
831 perform differential expression analysis with iDEP v0.91 workflow [87], a web
832 application that includes several conventional software applications such as DESeq2 [88]
833 and edgeR [89], and can perform comprehensive analysis of RNA-Seq data. After
834 normalizing all counts according to effective library size, we retained genes with > 1
835 count per million (CPM) in half of the samples (24 samples). A total of 13,608 genes
836 were then assessed in downstream analyses. Principal component analysis (PCA) was
837 first performed to reveal the overall expression pattern of each sample. While most
838 samples demonstrated distinct expression patterns, one supposed amygdala sample
839 (derived from a 4-month-old *Vmat1*$^{Thr/Thr}$ mouse) exhibited an expression pattern similar
840 to the other striatal samples (Supplementary Fig. S20). Given the inconsistency in the
841 expression pattern, we excluded this sample and conducted the normalization step again
842 for the remaining 47 samples.
843
844 **Differential expression and weighted gene correlation network analysis**
845 We conducted pair-wise between-genotype comparisons of the same brain regions to
846 identify differentially expressed genes (DEGs), which were defined by |log2(fold
847 change)| > 1 and false discovery rate (FDR; corrected by the Benjamini and Hochberg
848 method) < 0.05. The DEGs were further characterized by enrichment analysis for GO
849 terms in the iDEP pipeline. An Illumina BaseSpace application

850 (http://basespace.illumina.com/apps) was used to investigate the correlation in
851 expression levels of DEGs among currently and previously collected datasets. In this
852 analysis, we set FDR < 0.05 as cutoff to select genes for input, yielding 131 genes
853 recognized in total. To identify specific biological pathways affected by *Vmat1*
854 genotypes, we conducted weighted gene correlation network analysis (WGCNA) [90] of
855 15 samples from the amygdala. First, we calculated the transcripts per million (TPM)
856 for each gene, and the expression matrix was then adjusted for mouse batch as a
857 potential confounding factor. The 1000 genes with most variable expression levels
858 (largest coefficients of variation) among samples were retained. We chose a soft
859 thresholding power = 21, as it yielded a scale-free topology fitting index (R squared)
860 greater than 0.8. The correlations among gene expression levels across samples were
861 then calculated to detect co-expressing modules. We also calculated the correlations
862 between the expression levels of a given gene in the amygdala and the behavioral
863 composite (locomotor activity and anxiety), based on the data of 8 individuals (two for
864 each genotype). Genes belonging to modules of interest were further included in
865 protein-protein interaction networks constructed using STRING, and functional gene
866 clusters were detected by the MCODE module of Cytoscape 3.8.2 [91].
867

868 **Acknowledgments**

869 Some of the computations for transcriptomic analyses were performed on the NIG
870 supercomputer at ROIS National Institute of Genetics. We thank Dr. Liu Jinsha and Ms.
871 Eriko Koike for technical assistance with mouse embryo manipulations and care of
872 newborns, Ms. Chikako Ozeki and Tamaki Murakami for their assistance with
873 behavioral experiments, and Drs. Masayuki Koganezawa, Noriko Osumi and Leif
874 Andersson for their valuable comments on the manuscript.

875

876 **Funding**

877 This work was supported by the Japan Society for the Promotion of Science (Grants-in-
878 Aid for Scientific Research 17H05934 and 19H04892 to MK, 20J12055 to DXS,
879 17H05939 and 19H04897 to TS, 17H05967 and 19H04922 to YUI, and 16H06276 to
880 TM) and Intramural Research Grants for Neurological and Psychiatric Disorder of
881 NCNP (27-7, 30-9, and 3-9 to TI). This work was also supported by MEXT Promotion
882 of Distinctive Joint Research Center Program (Grant Number JPMXP0618217663).

883

884 **Availability of data and materials**

885 The datasets used and/or analyzed in the current study are available from the
886 corresponding author on reasonable request. The raw RNA-Seq reads have been
887 deposited in the NCBI Sequence Read Archive (SRA) under BioProject accession no.
888 PRJNA660500. Codes used for RNA-Seq analysis are available on the GitHub
889 repository: https://github.com/daikisato12/Vmat1_RNASeq.

890

891 **Authors' contributions**

892 DXS and MK conceived and DXS, YUI, SH, TK, and TS designed the study. DXS,
893 YUI, TI, TM, TS, and MK acquired funding. YUI and YM conducted genome-editing
894 experiments with mice. DXS, SH, KN, and TK designed and DXS and SH performed
895 behavioral tests. DXS analyzed behavioral test results with the help of SH and GS. NK
896 and TS performed electrophysiological and histological experiments. TS dissected all
897 the brain samples for RNA-Seq, for which DXS and HH performed data analysis. DXS,
898 YUI, TI, SH, TS, and MK wrote the manuscript with contributions and revisions from
899 all authors. All authors have read and approved the final manuscript.

900

901 **Ethical approval**

902 All animal care protocols and experiments were performed according to guidelines
903 approved by the Animal Care and Use Committee of the National Institute of
904 Neuroscience, National Center of Neurology and Psychiatry (approval numbers:
905 2017005, 2020007), the Animal Experiment Committee of Fujita Health University
906 (approval number: APU19063), and the Experimental Animal Ethics Committees of
907 Graduate School of Medicine, and the University of Tokyo (approval number: P29-14).

908

909 **Competing interests**

910 The authors declare no competing interests.

911

References

1. Sousa, A. M. M., Meyer, K. A., Santpere, G., Gulden, F. O. & Sestan, N. Evolution of the human nervous system function, structure, and development. *Cell* **170**, 226–247 (2017).
2. Raghanti, M. A. *et al.* A neurochemical hypothesis for the origin of hominids. *Proc. Natl. Acad. Sci. U. S. A.* **115**, E1108–E1116 (2018).
3. Zhu, Y. *et al.* Spatiotemporal transcriptomic divergence across human and macaque brain development. *Science* **362**, eaat8077 (2018).
4. Pryluk, R., Kfir, Y., Gelbard-Sagiv, H., Fried, I. & Paz, R. A tradeoff in the neural code across regions and species. *Cell* **176**, 1–13 (2019).
5. Cools, R., Roberts, A. C. & Robbins, T. W. Serotoninergic regulation of emotional and behavioural control processes. *Trends Cogn. Sci.* **12**, 31–40 (2008).
6. Shohamy, D. & Adcock, R. A. Dopamine and adaptive memory. *Trends Cogn. Sci.* **14**, 464–472 (2010).
7. Ebstein, R. P., Israel, S., Chew, S. H., Zhong, S. & Knafo, A. Genetics of human social behavior. *Neuron* vol. 65 831–844 (2010).
8. Sousa, A. M. M., Zhu, Y., Raghanti, M. A., Kitchen, R. R. & Onorati, M. Molecular and cellular reorganization of neural circuits in the human lineage. *Science* **358**, 1027–1032 (2017).
9. Canli, T. & Lesch, K. P. Long story short: The serotonin transporter in emotion regulation and social cognition. *Nature Neuroscience* vol. 10 1103–1109 (2007).

934 10. Bergey, C. M., Phillips-Conroy, J. E., Disotell, T. R. & Jolly, C. J. Dopamine
935 pathway is highly diverged in primate species that differ markedly in social
936 behavior. *Proc. Natl. Acad. Sci. U. S. A.* **113**, 6178–6181 (2016).
937 11. Rogers, J. The behavioral genetics of nonhuman primates: Status and prospects.
938 *Am. J. Phys. Anthropol.* **165**, 23–36 (2018).
939 12. Staes, N. *et al.* Serotonin receptor 1A variation is associated with anxiety and
940 agonistic behavior in chimpanzees. *Mol. Biol. Evol.* **36**, 1418–1429 (2019).
941 13. Sato, D. X. & Kawata, M. Positive and balancing selection on SLC18A1 gene
942 associated with psychiatric disorders and human-unique personality traits. *Evol.*
943 *Lett.* **2**, 499–510 (2018).
944 14. Erickson, J. D., Schäfer, M. K.-H., Bonner, T. I., Eiden, L. E. & Weihe, E.
945 Distinct pharmacological properties and distribution in neurons and endocrine
946 cells of two isoforms of the human vesicular monoamine transporter. *Proc. Natl.*
947 *Acad. Sci. U. S. A.* **93**, 5166–5171 (1996).
948 15. Lohr, K. M. *et al.* Increased vesicular monoamine transporter enhances dopamine
949 release and opposes Parkinson disease-related neurodegeneration in vivo. *Proc.*
950 *Natl. Acad. Sci. U. S. A.* **111**, 9977–82 (2014).
951 16. Lohoff, F. W. *et al.* Functional genetic variants in the vesicular monoamine
952 transporter 1 modulate emotion processing. *Mol. Psychiatry* **19**, 129–139 (2014).
953 17. Sato, D. X., Ishii, Y., Nagai, T., Ohashi, K. & Kawata, M. Human-specific
954 mutations in VMAT1 confer functional changes and multi-directional evolution
955 in the regulation of monoamine circuits. *BMC Evol. Biol.* **19**, 220 (2019).

956 18. Lohoff, F. W. *et al.* Variations in the vesicular monoamine transporter 1 gene
957 (VMAT1/SLC18A1) are associated with bipolar I disorder.
958 *Neuropsychopharmacology* **31**, 2739–2747 (2006).
959 19. Lohoff, F. W. *et al.* Association between variation in the vesicular monoamine
960 transporter 1 gene on chromosome 8p and anxiety-related personality traits.
961 *Neurosci. Lett.* **434**, 41–45 (2008).
962 20. Vaht, M., Kiive, E., Veidebaum, T. & Harro, J. A functional vesicular
963 monoamine transporter 1 (VMAT1) gene variant is associated with affect and the
964 prevalence of anxiety, affective, and alcohol use disorders in a longitudinal
965 population-representative birth cohort study. *Int. J. Neuropsychopharmacol.* **19**,
966 1–9 (2016).
967 21. Kim, B. *et al.* Dopamine D2 receptor-mediated circuit from the central amygdala
968 to the bed nucleus of the stria terminalis regulates impulsive behavior. *Proc.*
969 *Natl. Acad. Sci. U. S. A.* **115**, E10730–E10739 (2018).
970 22. Matthews, L. J. & Butler, P. M. Novelty-seeking DRD4 polymorphisms are
971 associated with human migration distance Out-of-Africa after controlling for
972 neutral population gene structure. **145**, 382–389 (2011).
973 23. Chen, J. Y., Wang, E. A., Cepeda, C. & Levine, M. S. Dopamine imbalance in
974 Huntington's disease: A mechanism for the lack of behavioral flexibility. *Front.*
975 *Neurosci.* **7**, 1–14 (2013).
976 24. Lohoff, F. W., Carr, G. V., Brookshire, B., Ferraro, T. N. & Lucki, I. Deletion of
977 the vesicular monoamine transporter 1 (vmat1/slc18a1) gene affects dopamine

978 signaling. *Brain Res.* **1712**, 151–157 (2019).

979 25. Enard, W. *et al.* Molecular evolution of FOXP2, a gene involved in speech and
980 language. *Nature* **418**, 869–872 (2002).

981 26. Enard, W. *et al.* A humanized version of Foxp2 affects cortico-basal ganglia
982 circuits in mice. *Cell* **137**, 961–971 (2009).

983 27. Carr, C. W. *et al.* Chiari I malformation, delayed gross motor skills, severe
984 speech delay, and epileptiform discharges in a child with FOXP1
985 haploinsufficiency. *Eur. J. Hum. Genet.* **18**, 1216–1220 (2010).

986 28. Hamdan, F. F. *et al.* De novo mutations in FOXP1 in cases with intellectual
987 disability, autism, and language impairment. *Am. J. Hum. Genet.* **87**, 671–678
988 (2010).

989 29. O'Roak, B. J. *et al.* Exome sequencing in sporadic autism spectrum disorders
990 identifies severe de novo mutations. *Nat. Genet.* **43**, 585–589 (2011).

991 30. Spiteri, E. *et al.* Identification of the transcriptional targets of FOXP2, a gene
992 linked to speech and language, in developing human brain. *Am. J. Hum. Genet.*
993 **81**, 1144–1157 (2007).

994 31. Vernes, S. C. *et al.* Foxp2 regulates gene networks implicated in neurite
995 outgrowth in the developing brain. *PLoS Genet.* **7**, e1002145 (2011).

996 32. Fong, W. L., Kuo, H. Y., Wu, H. L., Chen, S. Y. & Liu, F. C. Differential and
997 overlapping pattern of Foxp1 and Foxp2 expression in the striatum of adult
998 mouse brain. *Neuroscience* **388**, 214–223 (2018).

999 33. Wang, B., Lufkin, T. & Rubenstein, J. L. R. Dlx6 regulates molecular properties

1000 of the striatum and central nucleus of the amygdala. *J. Comp. Neurol.* **519**, 2320–
1001 2334 (2011).
1002 34. Ehrman, L. A. *et al.* The LIM homeobox gene Isl1 is required for the correct
1003 development of the striatonigral pathway in the mouse. *Proc. Natl. Acad. Sci. U.*
1004 *S. A.* **110**, E4027 (2013).
1005 35. Xu, Z. *et al.* SP8 and SP9 coordinately promote D2-type medium spiny neuron
1006 production by activating Six3 expression. *Development* **145**, (2018).
1007 36. Grundmann, S. *et al.* FoxP1 stimulates angiogenesis by repressing the inhibitory
1008 guidance protein semaphorin 5B in endothelial cells. *PLoS One* **8**, e70873
1009 (2013).
1010 37. O'Connor, T. P. *et al.* Semaphorin 5B mediates synapse elimination in
1011 hippocampal neurons. *Neural Dev.* **4**, 18 (2009).
1012 38. Brobey, R. K. *et al.* Klotho protects dopaminergic neuron oxidant-induced
1013 degeneration by modulating ASK1 and p38 MAPK signaling pathways. *PLoS*
1014 *One* **10**, e0139914 (2015).
1015 39. Sousa, K. M. *et al.* Wnt2 regulates progenitor proliferation in the developing
1016 ventral midbrain. *J. Biol. Chem.* **285**, 7246–7253 (2010).
1017 40. Multani, P. K. *et al.* VMAT1 deletion causes neuronal loss in the hippocampus
1018 and neurocognitive deficits in spatial discrimination. *Neuroscience* **232**, 32–44
1019 (2013).
1020 41. Revest, J. M. *et al.* Adult hippocampal neurogenesis is involved in anxiety-
1021 related behaviors. *Mol. Psychiatry* **14**, 959–967 (2009).

1022 42. Anacker, C. & Hen, R. Adult hippocampal neurogenesis and cognitive
1023 flexibility-linking memory and mood. *Nat. Rev. Neurosci.* **18**, 335–346 (2017).
1024 43. Adhikari, A., Topiwala, M. A. & Gordon, J. A. Synchronized Activity between
1025 the Ventral Hippocampus and the Medial Prefrontal Cortex during Anxiety.
1026 *Neuron* **65**, 257–269 (2010).
1027 44. Likhtik, E., Stujenske, J. M., Topiwala, M. A., Harris, A. Z. & Gordon, J. A.
1028 Prefrontal entrainment of amygdala activity signals safety in learned fear and
1029 innate anxiety. *Nat. Neurosci.* **17**, 106–113 (2014).
1030 45. Bukalo, O. *et al.* Prefrontal inputs to the amygdala instruct fear extinction
1031 memory formation. *Sci. Adv.* **1**, 1–9 (2015).
1032 46. Gabbott, P. L. A., Warner, T. A., Jays, P. R. L., Salway, P. & Busby, S. J.
1033 Prefrontal cortex in the rat: Projections to subcortical autonomic, motor, and
1034 limbic centers. *J. Comp. Neurol.* **492**, 145–177 (2005).
1035 47. Tye, K. M. *et al.* Amygdala circuitry mediating reversible and bidirectional
1036 control of anxiety. *Nature* **471**, 358–362 (2011).
1037 48. Janak, P. H. & Tye, K. M. From circuits to behaviour in the amygdala. *Nature*
1038 **517**, 284–292 (2015).
1039 49. de la Mora, M. P., Gallegos-Cari, A., Arizmendi-García, Y., Marcellino, D. &
1040 Fuxe, K. Role of dopamine receptor mechanisms in the amygdaloid modulation
1041 of fear and anxiety: Structural and functional analysis. *Prog. Neurobiol.* **90**, 198–
1042 216 (2010).
1043 50. Hansson, S. R., Hoffman, B. J. & Mezey, É.´. Ontogeny of vesicular monoamine

1044 transporter mRNAs VMAT1 and VMAT2. I. The developing rat central nervous
1045 system. *Dev. Brain Res.* **110**, 135–158 (1998).
1046 51. Murray, E. A. The amygdala, reward and emotion. *Trends Cogn. Sci.* **11**, 489–
1047 497 (2007).
1048 52. Posner, J. *et al.* Alterations in amygdala-prefrontal circuits in infants exposed to
1049 prenatal maternal depression. *Transl. Psychiatry* **6**, e935 (2016).
1050 53. Chang, X. *et al.* RNA-seq analysis of amygdala tissue reveals characteristic
1051 expression profiles in schizophrenia. *Transl. Psychiatry* **7**, e1203 (2017).
1052 54. Avino, T. A. *et al.* Neuron numbers increase in the human amygdala from birth
1053 to adulthood, but not in autism. *Proc. Natl. Acad. Sci. U. S. A.* **115**, 3710–3715
1054 (2018).
1055 55. Asari, T. *et al.* Amygdalar enlargement associated with unique perception.
1056 *Cortex* **46**, 94–99 (2010).
1057 56. Rice, K., Viscomi, B., Riggins, T. & Redcay, E. Amygdala volume linked to
1058 individual differences in mental state inference in early childhood and adulthood.
1059 *Dev. Cogn. Neurosci.* **8**, 153–163 (2014).
1060 57. Bickart, K. C., Wright, C. I., Dautoff, R. J., Dickerson, B. C. & Barrett, L. F.
1061 Amygdala volume and social network size in humans. *Nat. Neurosci.* **14**, 163–
1062 164 (2011).
1063 58. Sallet, J. *et al.* Social network size affects neural circuits in Macaques. *Science*
1064 **334**, 697–700 (2011).
1065 59. Atzil, S. *et al.* Dopamine in the medial amygdala network mediates human

1066 bonding. *Proc. Natl. Acad. Sci. U. S. A.* **114**, 2361–2366 (2017).

1067 60. Bickart, K. C., Dickerson, B. C. & Barrett, L. F. The amygdala as a hub in brain
1068 networks that support social life. *Neuropsychologia* **63**, 235–248 (2014).

1069 61. Schreiweis, C. *et al.* Humanized Foxp2 accelerates learning by enhancing
1070 transitions from declarative to procedural performance. *Proc. Natl. Acad. Sci. U.*
1071 *S. A.* **111**, 14253–14258 (2014).

1072 62. Zhu, F., Nair, R. R., Fisher, E. M. C. & Cunningham, T. J. Humanising the
1073 mouse genome piece by piece. *Nat. Commun.* **10**, 1845 (2019).

1074 63. Wray, N. R. *et al.* Genome-wide association analyses identify 44 risk variants
1075 and refine the genetic architecture of major depression. *Nat. Genet.* **50**, 668–681
1076 (2018).

1077 64. Ripke, S. *et al.* Biological insights from 108 schizophrenia-associated genetic
1078 loci. *Nature* (2014) doi:10.1038/nature13595.

1079 65. Lo, M. T. *et al.* Genome-wide analyses for personality traits identify six genomic
1080 loci and show correlations with psychiatric disorders. *Nat. Genet.* **49**, 152–156
1081 (2017).

1082 66. Lohoff, F. W. *et al.* Association between polymorphisms in the vesicular
1083 monoamine transporter 1 gene (VMAT1/SLC18A1) on chromosome 8p and
1084 schizophrenia. *Neuropsychobiology* **57**, 55–60 (2008).

1085 67. Löytynoja, A. & Goldman, N. webPRANK: a phylogeny-aware multiple
1086 sequence aligner with interactive alignment browser. *BMC Bioinformatics* **11**,
1087 579 (2010).

1088 68. Minh, B. Q. *et al.* IQ-TREE 2: new models and efficient methods for
1089 phylogenetic inference in the genomic era. *Mol. Biol. Evol.* **37**, 1530–1534
1090 (2020).
1091 69. Letunic, I. & Bork, P. Interactive Tree of Life (iTOL) v4: Recent updates and
1092 new developments. *Nucleic Acids Res.* **47**, 256–259 (2019).
1093 70. Waterhouse, A. *et al.* SWISS-MODEL: homology modelling of protein
1094 structures and complexes. *Nucleic Acids Res.* **46**, W296–W303 (2018).
1095 71. Choi, Y. & Chan, A. P. PROVEAN web server: a tool to predict the functional
1096 effect of amino acid substitutions and indels. *Bioinformatics* **31**, 2745–2747
1097 (2015).
1098 72. Kumar, P., Henikoff, S. & Ng, P. C. Predicting the effects of coding non-
1099 synonymous variants on protein function using the SIFT algorithm. *Nat. Protoc.*
1100 **4**, 1073–1081 (2009).
1101 73. Rodrigues, C. H. M., Pires, D. E. V. & Ascher, D. B. DynaMut: predicting the
1102 impact of mutations on protein conformation, flexibility and stability. *Nucleic*
1103 *Acids Res.* **46**, W350–W355 (2018).
1104 74. Concordet, J. P. & Haeussler, M. CRISPOR: Intuitive guide selection for
1105 CRISPR/Cas9 genome editing experiments and screens. *Nucleic Acids Res.* **46**,
1106 W242–W245 (2018).
1107 75. Hashimoto, M., Yamashita, Y. & Takemoto, T. Electroporation of Cas9
1108 protein/sgRNA into early pronuclear zygotes generates non-mosaic mutants in
1109 the mouse. *Dev. Biol.* **418**, 1–9 (2016).

1110 76. Miyakawa, T., Yamada, M., Duttaroy, A. & Wess, J. Hyperactivity and intact
1111 hippocampus-dependent learning in mice lacking the M1 muscarinic
1112 acetylcholine receptor. *J. Neurosci.* **21**, 5239–5250 (2001).
1113 77. Takao, K. & Miyakawa, T. Light/dark transition test for mice. *J. Vis. Exp.* **1**,
1114 e104 (2006).
1115 78. Takao, K. *et al.* Comprehensive behavioral analysis of calcium/calmodulin-
1116 dependent protein kinase IV knockout mice. *PLoS One* **5**, e9460 (2010).
1117 79. Komada, M., Takao, K. & Miyakawa, T. Elevated plus maze for mice. *J. Vis.*
1118 *Exp.* **22**, e1088 (2008).
1119 80. Shoji, H., Hagihara, H., Takao, K., Hattori, S. & Miyakawa, T. T-maze forced
1120 alternation and left-right discrimination tasks for assessing working and reference
1121 memory in mice. *J. Vis. Exp.* **60**, e3300 (2012).
1122 81. Miyakawa, T. *et al.* Conditional calcineurin knockout mice exhibit multiple
1123 abnormal behaviors related to schizophrenia. *Proc. Natl. Acad. Sci. U. S. A.* **100**,
1124 8987–8992 (2003).
1125 82. Kline, R. B. *Principles and Practice of Structural Equation Modeling*.
1126 *Methodology in the social sciences* (The Guilford Press, 2016).
1127 83. Palkovits, M. & Brownstein, M. J. *Maps and guide to microdissection of the rat*
1128 *brain*. (Elsevier Science Publ. Co., 1988).
1129 84. Chen, S., Zhou, Y., Chen, Y. & Gu, J. fastp: an ultra-fast all-in-one FASTQ
1130 preprocessor. *Bioinformatics* **34**, i884–i890 (2018).
1131 85. Dobin, A. *et al.* STAR: ultrafast universal RNA-seq aligner. *Bioinformatics* **29**,

1132 15–21 (2013).

1133 86. Liao, Y., Smyth, G. K. & Shi, W. featureCounts: an efficient general purpose
1134 program for assigning sequence reads to genomic features. *Bioinformatics* **30**,
1135 923–930 (2014).

1136 87. Ge, S. X., Son, E. W. & Yao, R. iDEP: An integrated web application for
1137 differential expression and pathway analysis of RNA-Seq data. *BMC*
1138 *Bioinformatics* **19**, 1–24 (2018).

1139 88. Love, M. I., Huber, W. & Anders, S. Moderated estimation of fold change and
1140 dispersion for RNA-seq data with DESeq2. *Genome Biol.* **15**, 550 (2014).

1141 89. Robinson, M. D., McCarthy, D. J. & Smyth, G. K. edgeR: a Bioconductor
1142 package for differential expression analysis of digital gene expression data.
1143 *Bioinformatics* **26**, 139–140 (2010).

1144 90. Langfelder, P. & Horvath, S. WGCNA: An R package for weighted correlation
1145 network analysis. *BMC Bioinformatics* **9**, 559 (2008).

1146 91. Shannon, P. *et al.* Cytoscape: a software environment for untegrated models.
1147 *Genome Res.* **13**, 2498–2504 (2003).

1148

1149

1150 **Tables and Figures**

1151 **Table 1. *In silico* prediction of mVMAT1 tolerance to the humanized mutations**

1152 **Asn133Thr and Asn133Ile.** Text in bold indicates significant effects of the

1153 substitutions as predicted by Provean score < –2.5 or SIFT score < 0.05. The Provean

1154 term "Deleterious" and SIFT term "Damaging" refer to significant effects on protein

1155 function but do not necessarily indicate that they deteriorate protein function. All three

1156 methods predict that 133Ile has greater effects than 133Thr on mVMAT1 function.

Ref.	Alt.	Provean		SIFT		DynaMut	
		Score	Prediction	Score	Prediction	ΔΔG (kcal/mol)	Prediction
Asn	Thr	**-3.27**	**Deleterious**	0.243	Tolerated	-0.062	Destabilizing
Asn	Ile	**-6.55**	**Deleterious**	**0.014**	**Damaging**	1.106	Stabilizing

1157

1158

1159 **Table 2. List of gene ontology (GO) terms significantly overrepresented in the set**

1160 **of differentially expressed genes (DEGs) between *Vmat1*^{WT} and *Vmat1*$^{Ile/Ile}$ mice.**

1161 *P* values were corrected by the Benjamini-Hochberg method. Only terms with $P < 0.05$

1162 are presented. Downregulation indicates *Vmat1*^{WT} > *Vmat1*$^{Ile/Ile}$ while upregulation

1163 indicates *Vmat1*$^{Ile/Ile}$ > *Vmat1*^{WT}.

Direction	Pathways	Genes	adj.Pval
Upregulated	Regulation of cell junction assembly	*Ace*, *Cldn1*, *Enpp2*	5.5×10^{-3}
Downregulated	Locomotory behavior	*Gng7*, *Gpr88*, *Ido1*, *Pde1b*, *Penk*, *Ppp1r1b*, *Rasd2*	7.2×10^{-5}
Downregulated	Behavior	*Asic4*, *Foxp1*, *Gng7*, *Gpr88*, *Ido1*, *Pde1b*, *Penk*, *Ppp1r1b*, *Rasd2*	4.9×10^{-4}
Downregulated	Mononuclear cell differentiation	*Cd4*, *Foxp1*, *Pde1b*	2.8×10^{-3}
Downregulated	Response to amphetamine	*Pde1b*, *Ppp1r1b*, *Rgs9*	2.8×10^{-3}
Downregulated	Multicellular organismal response to stress	*Asic4*, *Gng7*, *Ido1*, *Penk*	2.8×10^{-3}
Downregulated	Cardiac muscle tissue development	*Foxp1*, *Myom3*, *Rarb*, *Rbp4*, *Wnt2*	3.9×10^{-3}
Downregulated	Regulation of cardiac muscle cell proliferation	*Foxp1*, *Rbp4*, *Wnt2*	4.0×10^{-3}
Downregulated	Behavioral fear response	*Asic4*, *Gng7*, *Penk*	4.6×10^{-3}
Downregulated	cAMP catabolic process	*Pde7b*, *Pde10a*	4.8×10^{-3}

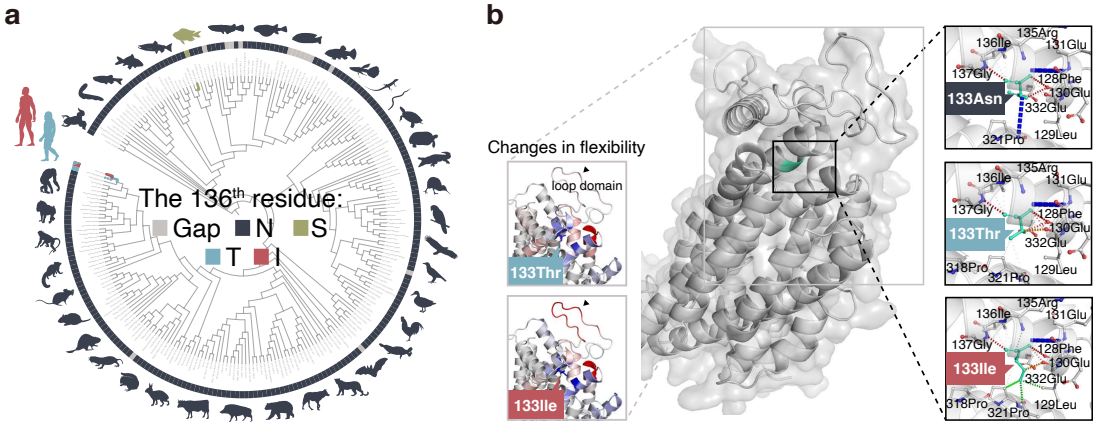

Figure 1. An ultra-conserved residue in VMAT1 exhibits functional variants unique to humans. (a) A phylogenetic tree constructed by multiple sequence alignment of the *VMAT1* gene. Almost all genes across 236 vertebrate species retain asparagine (N, Asn) on the 136th residue, while humans are the only vertebrate species except for bicolor damselfish (shown in green) with a unique polymorphism (T/I, Thr136Ile; rs1390938). Note that the phylogenetic relationship presented here is not necessarily consistent with the known species tree. **(b)** mVMAT1 protein structure predicted by homology modeling and the effects of human-type mutagenesis (corresponding to 133Thr and 133Ile in mVMAT1). (Left) Δ Vibrational entropy energy between WT (133Asn) and mutants. Amino acids are colored according to the vibrational entropy change conferred by the given mutation. Red represents a gain of flexibility and blue represents a rigidification of the structure. The 133Ile mutation leads to increased flexibility of the first luminal loop, a receptor-like domain affecting the affinity of ligands. (Right) When introduced *in silico*, 133Ile but not 13Thr exhibits hydrophobic interactions (shown by green dotted line) with surrounding sites, which likely influence the folding and/or stability of mVMAT1 protein. Blue, red, and orange dotted lines

represent amide bonds, hydrogen bonds, and weak van der Waals interactions, respectively.

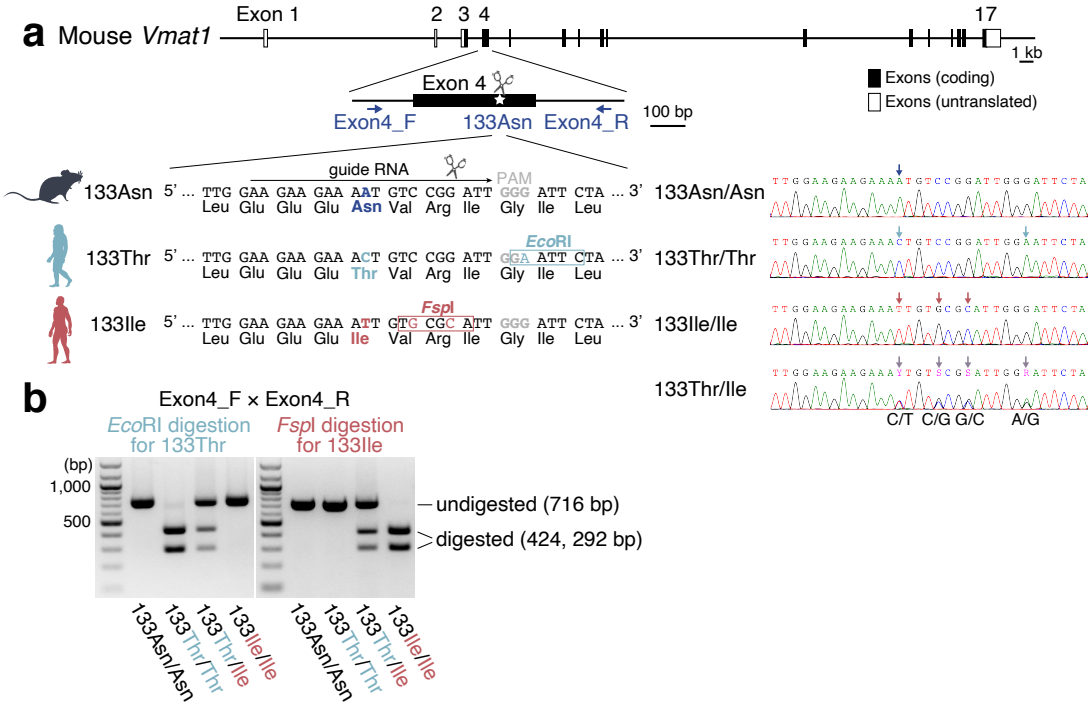

1184

1185 **Figure 2. Generation of the *Vmat1*-humanized mouse models by CRISPR/Cas9**

1186 **genome editing. (a)** Targeting strategy for mVMAT1 133Asn humanization. Genetic

1187 configuration of the mouse *Vmat1* gene is shown above. Exon 4 encoding 133Asn is

1188 enlarged, and the primers used for genotyping (Exon4_F and Exon4_R) are depicted.

1189 To replace the mouse 133Asn with 133Thr or 133Ile by CRISPR/Cas9-mediated

1190 genome engineering, a guide RNA with minimum off-target effects was designed. GGG

1191 (gray) represents the PAM sequence. In addition to 133Asn humanization, restriction

1192 enzyme recognition sites (*Eco*RI and *Fsp*I) were synonymously incorporated to avoid

1193 the unwanted re-editing and to simplify genotyping. Sanger sequencing profiles of

1194 133Asn/Asn (WT), 133Thr/Thr, 133Ile/Ile, and 133Thr/Ile are shown on the right. **(b)**

1195 PCR-RFLP assay, in which PCR products amplified using Exon4_F and Exon4_R were

1196 digested by *Eco*RI and *Fsp*I, respectively, could be used to distinguish 4 genotypes

1197 without sequencing.

1198

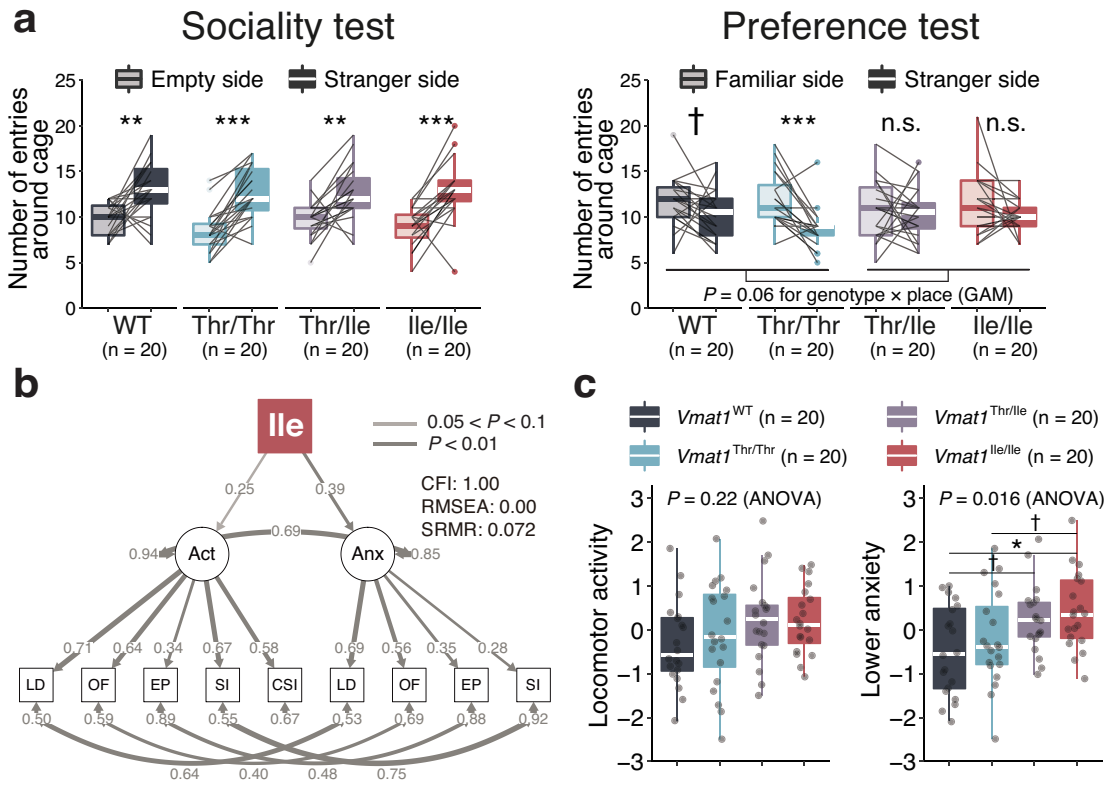

Figure 3. Comprehensive behavioral tests reveal distinct behavioral changes in *Vmat1*$^{Thr/Thr}$ and *Vmat1*^{Ile} mice, including reduced anxiety. (a) In Crawley's social interaction test, *Vmat1*$^{Thr/Thr}$ mice preferred a familiar (previously exposed) mouse over a novel stranger. **(b)** Structural Equation Modeling (SEM) revealed the best fit model to explain the effects of *Vmat1* genotype on locomotor activity (Act) and anxiety (Anx). According to the model, *Vmat1*^{Ile} (*Vmat1*$^{Thr/Ile}$ and *Vmat1*$^{Ile/Ile}$) significantly reduces anxiety-like behavior. The boxes and circles represent measured and latent variables, respectively. The paths represent causal relationships on which numerical values indicate standardized coefficient and the gray-scale intensity of the paths indicates statistical significance tested by *t*-test. See Methods for the detailed modeling procedure. **(c)** *Vmat1*^{Ile} mice exhibited lower anxiety than WT and *Vmat1*$^{Thr/Thr}$

genotypes. See Methods for the detailed calculation of the scores. For the composite anxiety score, a higher value indicates lower anxiety. Statistical significance was evaluated by paired *t*-test for **(a),** and by pair-wise *t*-test with FDR correction by the Benjamini-Hochberg method for **(c)**. Interactive effects of genotype (Ile allele labeled by 1, and 0 otherwise) and cage place were also assessed by generalized additive model with quasi-Poisson distribution in **(a)**. †: $0.05 < P < 0.1$, *: $0.01 < P < 0.05$, **: $0.001 < P < 0.01$, ***: $P < 0.001$.

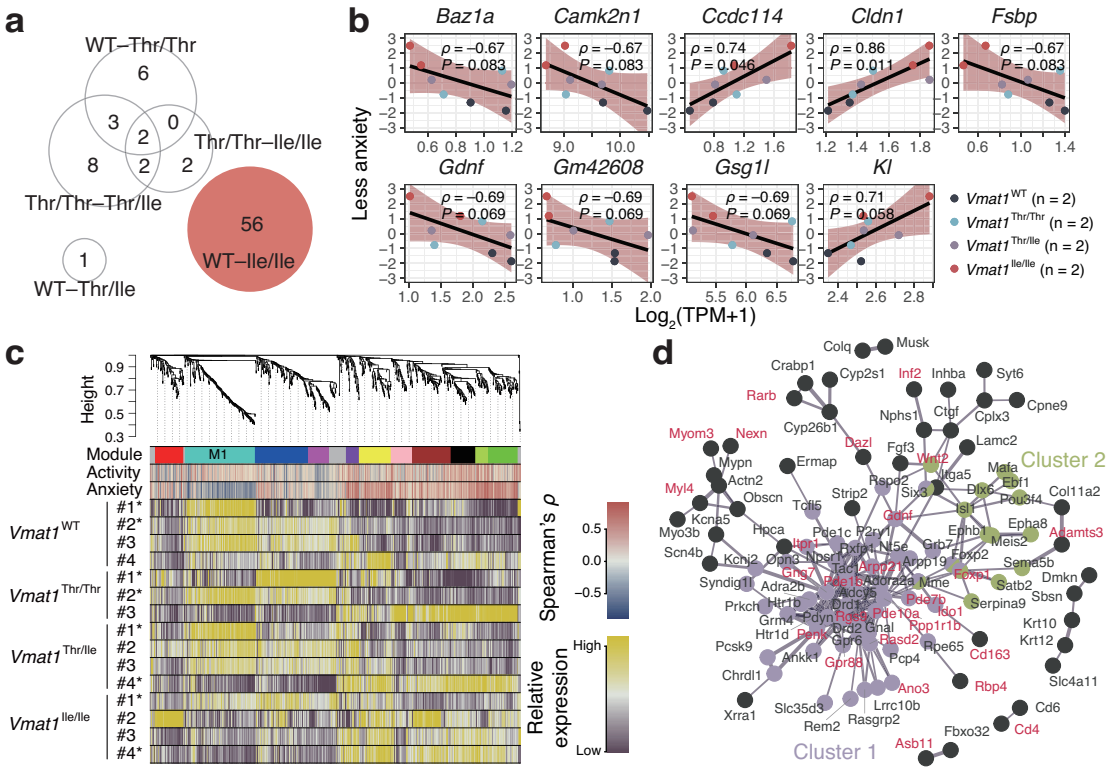

Figure 4. Differentially expressed genes (DEGs) in the brain among *Vmat1* genotypes and predicted co-expressing modules. **(a)** The number of DEGs detected by pair-wise comparisons among the four genotypes. All DEGs were found in the amygdala (with none in prefrontal cortex or striatum). **(b)** Correlations between individual DEG expression levels for the WT vs. and *Vmat1*$^{\text{Ile/Ile}}$ comparison and composite anxiety scores from LD, EP, OF, and SI tests (see Methods). Only genes with strong Spearman's correlations ($P < 0.1$) are shown. The bands are 95% confidence intervals. **(c)** Network dendrogram from co-expression modules based on the expression data of all 47 regional brain samples. Each branch represents an individual gene, and the colors below represent the module, correlation (ρ) with behavioral phenotype (locomotor activity and anxiety), and the relative expression level in the amygdala across genotypes. The samples with asterisks are from mice with behavioral data and

1232 were used to calculate the correlations between expression levels and behavioral

1233 phenotypes. The M1 module (shown in turquoise), showing negative correlations with

1234 anxiety score exhibited significant overrepresentation of the DEGs detected between

1235 WT and *Vmat1*$^{Ile/Ile}$ mice. **(d)** Protein–protein interaction networks among the genes in

1236 M1. The DEGs detected between WT and *Vmat1*$^{Ile/Ile}$ mice are shown in red. The

1237 thickness of the line indicates the strength of data support analyzed by STRING.

1238

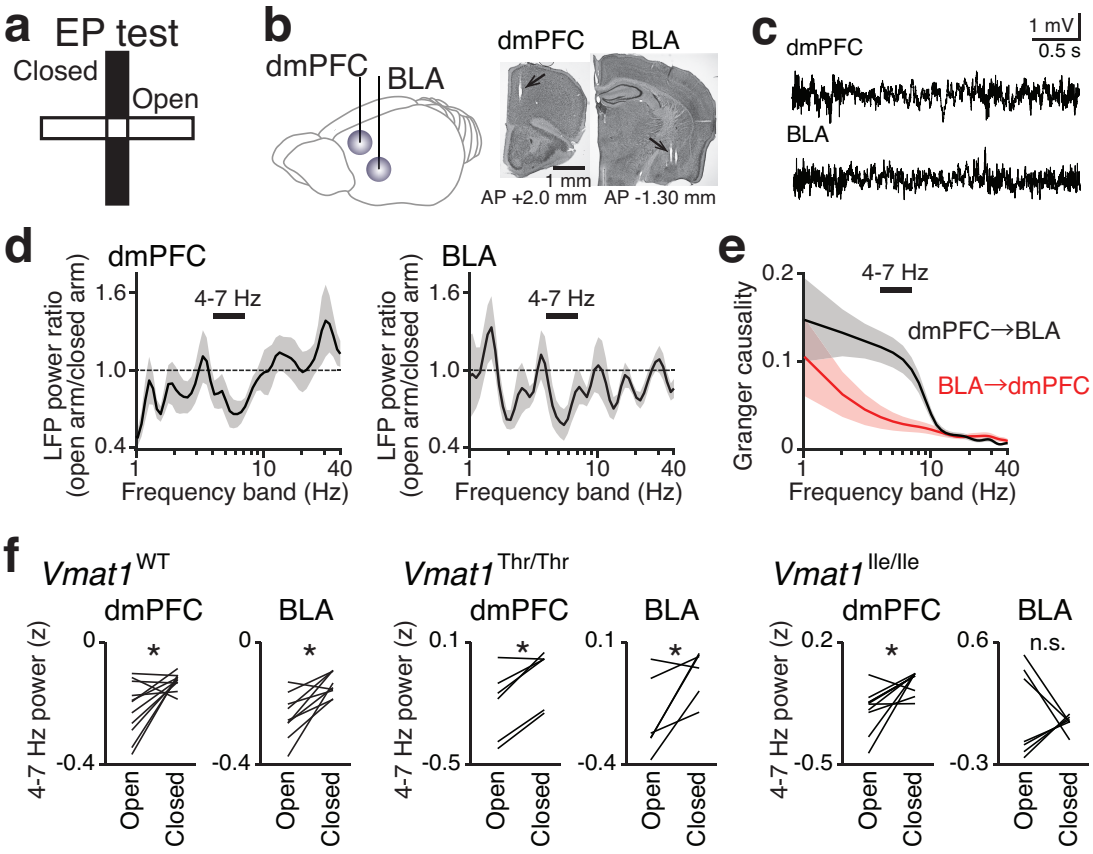

Figure 5. Wild-type and *Vmat1*$^{Thr/Thr}$ mice, but not *Vmat1*$^{Ile/Ile}$ mice, exhibit a reduction in amygdalar 4–7 Hz local field potential (LFP) power under anxiogenic conditions. (a) (Left) LFP recordings were simultaneously performed from the dorsomedial prefrontal cortex (dmPFC) and basolateral amygdala (BLA). (Right) Histological confirmation of electrode locations in the dmPFC and BLA. **(b)** Typical LFP signals from the dmPFC and BLA. **(c)** An elevated plus maze (EP) test. **(d)** Spectrograms of dmPFC (left) and BLA (right) LFP power in (anxiogenic) open arms relative to closed arms. Data were averaged from all *Vmat1*^{WT} mice. The bar above indicates the 4–7 Hz band, showing pronounced decreases in LFP power in both regions. **(e)** Spectral Granger causality averaged over 20 dmPFC–BLA electrode pairs.

1250 **(f)** Comparison of dmPFC and BLA LFP 4–7 Hz power (z-scored) between open and

1251 closed arms. *$P < 0.05$, paired *t*-test. Each line represents one electrode.

1252